An analysis of the optical response of amorphous semiconductors with distributions of defect states

by

Shamsul Azam Chowdhury

B.Sc., Bangladesh University of Engineering and Technology (BUET), 2009

A THESIS SUBMITTED IN PARTIAL FULFILLMENT OF
THE REQUIREMENTS FOR THE DEGREE OF

MASTER OF SCIENCE

in

THE COLLEGE OF GRADUATE STUDIES

(Electrical Engineering)

THE UNIVERSITY OF BRITISH COLUMBIA

(Okanagan)

February 2014

Abstract

Defects play an important role in shaping the optical response of a semiconductor material. In this thesis, models for the spectral dependence of the imaginary part of the dielectric function, for the specific case of defective amorphous semiconductors, are considered. Within the framework of a joint density of states functional analysis, closed-form expressions are derived for the imaginary part of the dielectric function, with defect states taken into account. Both valence band and conduction band defect models are considered in this analysis. The role that the different types of optical transitions play in shaping the corresponding optical response are also closely examined. Using the derived models, the spectral dependence of the optical absorption coefficient is compared with that of experiment for defect absorption influenced samples of amorphous silicon. The fits of these models with the results of experiment are found to be satisfactory.

Table of Contents

List of Tables

List of Figures

List of Symbols

$\mathcal{R}^2(E)$	aggregate dipole matrix element squared average
$\mathcal{P}^2(E)$	aggregate momentum matrix element squared average
γ_v	breadth of the valence band tail
γ_c	breadth of the conduction band tail
$\gamma_{v_{\mathbf{D}}}$	breadth of the valence band defect distribution
$\gamma_{c_{\mathbf{D}}}$	breadth of the conduction band defect distribution
E_c	conduction band band edge
N_{co}	conduction band density of states prefactor
N^*_{co}	conduction band tail prefactor
$N_c(E)$	conduction band density of states function
$E_{v_{\mathbf{T}}}$	critical energy at which the exponential and square-root distributions interface in the valence band
$E_{v_{\mathbf{D}}}$	critical energy at which the exponential and defect distributions interface in the valence band

$E_{c_{\mathbf{T}}}$	critical energy at which the exponential and square-root distributions interface in the conduction band
$E_{c_{\mathbf{D}}}$	critical energy at which the exponential and defect distributions interface in the conduction band
ρ_A	density of silicon atoms
q	electron charge
m_e	electron mass
E_g	energy gap
E_F	Fermi energy level
$\mathcal{V}$	illuminated volume
ϵ_2	imaginary part of the dielectric function
$I(z)$	intensity of light at position z
I_0	intensity of light at position z=0
α	optical absorption coeffieient
E	Photon energy
$n(E)$	Refractive index
$\|v\rangle$	single spin electronic state associated with the valence band
$\|c\rangle$	single spin electronic state associated with the conduction band
E_v	valance band band edge
N_{vo}	valence band density of states prefactor

$N_v(E)$	valence band density of states function
N_{vo}^*	valence band tail prefactor

List of Acronyms

a-Si	amorphous silicon
c-Si	crystalline silicon
DOS	density of States
JDOS	joint density of states
VBB	valence band band
VBT	valence band tail
VBD	valence band defect
CBB	conduction band band
CBT	conduction band tail
CBD	conduction band defect

Acknowledgements

This thesis would not have been possible without the help and support of my colleagues, friends, and family.

I am heartily thankful to my supervisor, Dr. Stephen O'Leary, for both inspiring and teaching me. His constant guidance, support and encouragement helped me throughout my thesis.

To my family

Chapter 1

Introduction

The semiconductor industry, as we know it today, can trace its origins back to a series of innovations that occurred in the mid-20th Century at Bell Telephone Laboratories in Murray Hill, New Jersey. By that time, vacuum tube technology had been fully developed, and such tubes were deployed in all aspects of the telephone network; vacuum tubes were then used in order to electronically process electrical signals. Electro-mechanical relays, allowing for automatic telephone dialing and switching over such networks, were also available and also widely deployed. Thus, at the time, to the technical lay-person at least, it may have appeared that the technology was available in order to address all communication needs for the foreseeable future.

As far as the management of Bell Telephone Laboratories was concerned, however, difficulties still persisted. Vacuum tubes consume large amounts of electrical power and have a relatively short mean-time-to-failure. Electro-

mechanical relays, while offering many enticing capabilities, operated at limited speeds. In addition, they were also inherently prone to failure. There was a realization that the limitations inherent to these technologies would eventually limit future developments in telephony. Thus, a group was commissioned in 1945 in order to find a solid-state alternative to both vacuum tubes and electro-mechanical relays that will offer the same functionality but at a reduced cost and with greater reliability. This group, led by the brilliant but mercurially tempered William B. Shockley, focused upon a class of hitherto unexplored materials, semiconductors, owing to their peculiar and promising properties. This effort paid off handsomely in short order, the demonstration of the first semiconductor-based transistor occurring on Christmas Eve of 1947.

The developments in electronics that have occurred since that time have primarily arisen as a consequence of a detailed and quantitative understanding of the material properties of the materials used within the constituent electron devices found within electronic systems. As a consequence, the material properties of conductors, insulators, and dielectrics, the materials from which these constituent electron devices are fabricated, has been the focus of tremendous interest for many years. This understanding has allowed for a shrinking in the dimensions of these electron devices as well as a

concomitant increase in the number of electron devices packed onto a given chip. In fact, in 1965, Gordon E. Moore, the founding president of Intel, suggested that the number of transistors on a given chip would double every 18 months for the next decade; see Figure 1.1 [1]. Moore's law, as this 1965 projection is now referred to as, has held for almost 5 decades now, and the present expectation is that it will continue to hold for at least another decade. As the dimensions of the devices employed approach fundamental limits, however, it is clear that a deeper understanding of the material properties of these materials will be required if Moore's law is to continue to hold into the future. As a consequence, research into the material properties of semiconductors continues with great intensity.

Progress in conventional electronics has typically been achieved by making the constituent electron devices smaller, faster, more reliable, and less expensive. There is, however, another class of electron device that requires size in order to be useful. Scanners and displays, which act at the interface between the human world and its digital counterpart, must be of a certain size in order to perform properly. Solar cells and x-ray imagers also must be of a certain size in order to perform properly. These devices are all referred to as examples of large area electronic devices.

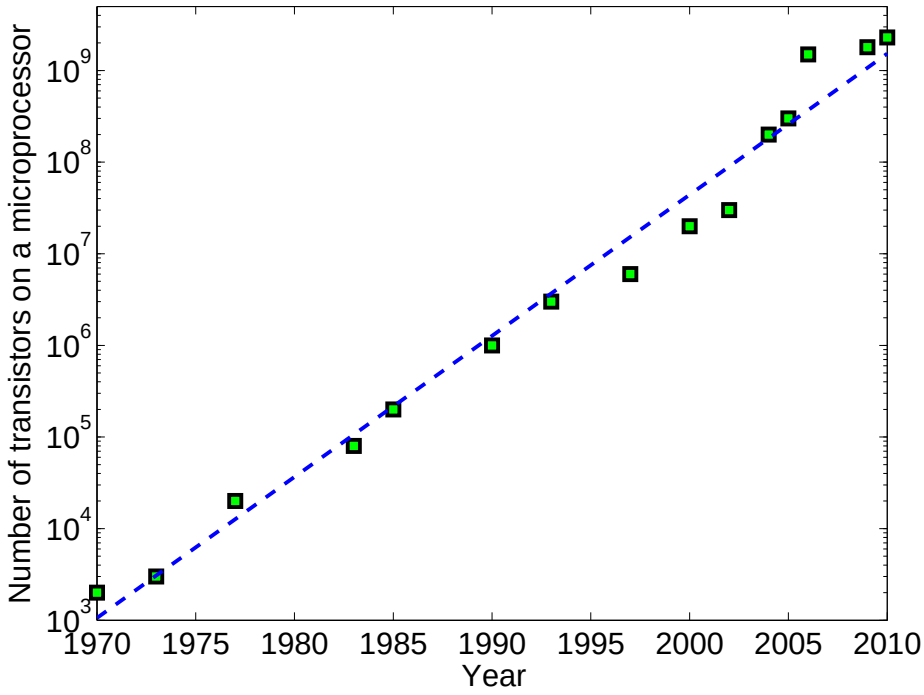

Figure 1.1: The number of transistors on a microprocessor. This figure is after Hadi [1].

Starting off as a niche field of inquiry in the late 1960s, large area electronics is now an important field in its own right, with commercial sales now constituting a substantial fraction of the overall commercial semiconductor market; see Figure 1.2 [2]. While the focus in conventional electronics is on fabricating devices with sub-micron device features, in large area electronics the focus instead is on depositing thin-films uniformly and inexpensively over substrates of the order of a square-meter in dimensions [3]. Crystalline silicon (c-Si), the dominant material used in conventional electronics, can not be used as a material for thin-film deposition, and thus, other materials must be used instead. Amorphous silicon (a-Si) and microcrystalline silicon (μc-Si) are often used for this purpose. As they are disordered forms of silicon, the electronic properties of these materials are rather distinct from those of their crystalline counterparts. It is the quantitative understanding of these differences that has been the focus of materials work for a great many years.

For many of the device applications considered within the large area electronics field, the response of the underlying electronic materials to light plays a decisive role in determining the corresponding device performance. This is particularly true for solar cell devices and digital flat panel x-ray image detectors, the response to light being a fundamental performance

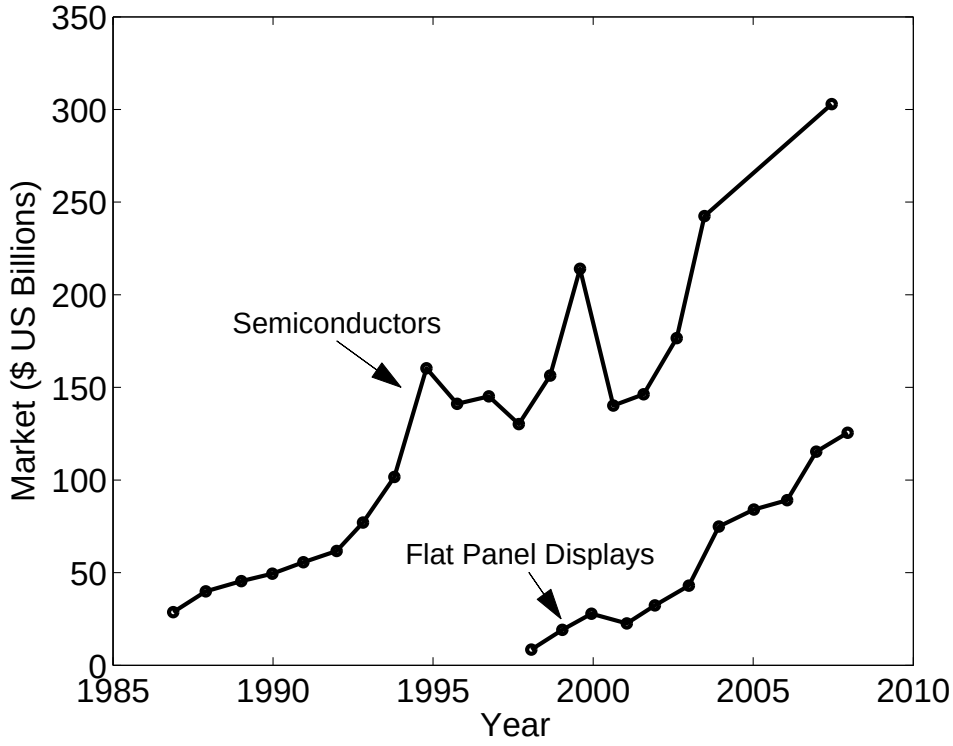

Figure 1.2: Semiconductor and flat panel display shipments, plotted as a function of date. This data was obtained from the 2005 Information Society Technologies proposal for advancement [2].

metric associated with both applications. Accordingly, the optical response of the materials used within large area electron devices continues to be an important focus of research.

When a material is exposed to light, i.e., when light passes through a given material, the intensity of the light decreases with the depth into the material. Consider, for example, a beam of light perpendicularly incident upon a semi-infinite slab of a material, as depicted in Figure 1.3 [4]. If the material properties are uniform, as the light passes through the material, its intensity will diminish exponentially. In the absence of reflections from the surface of the material, the intensity of the beam of light within the material can be expressed as a function of the penetration depth into the material, z, i.e.,

$$I(z) = I_o \exp(-\alpha z), \tag{1.1}$$

where I_o denotes the intensity of the light at the surface of the material, $z = 0$, and α represents the optical absorption coefficient [5]. The optical absorption coefficient, α, determines how far light can penetrate into a material before it is fully absorbed. This coefficient exhibits a strong spectral dependence on the incident photon energy, E, and from this dependence, the nature of the optical transitions that occur within the semiconductor may be determined.

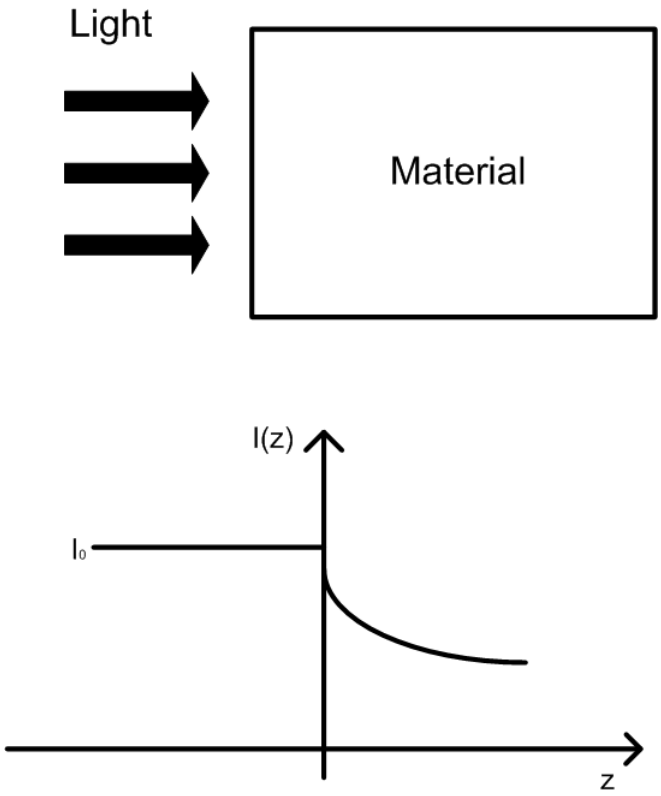

Figure 1.3: A schematic depiction of the light intensity as a function of the penetration depth, z. It is assumed that the interface between the vacuum and the material is at $z = 0$, and that the incident light propagates from the left. Reflections from the surface are neglected. This figure is after Thevaril [4].

The experimental determination of the spectral dependence of the optical absorption coefficient, i.e., the determination of $\alpha(E)$, will allow one to determine: (1) the energy gap of the material, (2) the nature of this energy gap, i.e., whether it be direct or indirect, and (3) provide some insights into the amount of disorder that is present within the material. With reference to the third point mentioned, it should be noted that in a disorderless crystalline semiconductor, at zero-temperature, this optical absorption spectrum terminates abruptly at the energy gap, while in an amorphous or microcrystalline semiconductor, the optical absorption spectrum will encroach into the otherwise empty gap region, the amount of encroachment corresponding to how much disorder is present. From a detailed study into the nature of this encroachment, insights into the character of the underlying distributions of electronic states may be gleaned.

In this thesis, an empirical model for the distribution of electronic states associated with an amorphous semiconductor, which includes defect states, will be developed, and the corresponding spectral dependence of the optical absorption spectrum will be determined. The distribution of defect states within an amorphous semiconductor will be modeled by adding broad exponential tails of defect states onto a traditional model for the distribution of electronic states in the absence of defect states. The corresponding op-

tical absorption spectrum is then determined through an evaluation of the corresponding joint density of states (JDOS) function, this being obtained through a convolution over the valence band and conduction band distributions of electronic states and the use of a model for the relationship between the spectral dependence of the imaginary part of the dielectric function and that of the corresponding JDOS function. The results of these theoretical investigations are then compared with those of experiment, and from this comparison, the modeling parameters are determined. For the purposes of this analysis, the primary focus is on the case of hydrogenated amorphous silicon (a-Si:H), the most widely deployed amorphous semiconductor today.

This thesis is organized in the following manner. In Chapter 2, the theoretical background for this analysis is presented. Then, in Chapter 3, a model for the distribution of electronic states, one which includes treatment of the distributions of defect states, is introduced. The resultant spectral dependence of the optical absorption coefficient, $\alpha(E)$, is then evaluated in Chapter 4, a comparison with the results of experiment, for the specific case of a-Si:H, being provided. Finally, the conclusions of this analysis, and some recommendations for further research, are presented in Chapter 5.

Chapter 2

Background material

2.1 The optical response

The response of a given material to light, i.e., its optical response, is often considered in materials characterization studies. Optical transitions, from occupied valence band electronic states to unoccupied conduction band electronic states, determine the nature of this response. The distribution of electronic states, the occupancy of these states, and the probability that a given optical transition between such states can occur at all, play roles in shaping the exact form of this response. The central goal of this analysis is to develop a model for the spectral dependence of the optical absorption coefficient, $\alpha(E)$, that may be used in order to interpret the physical meaning of the optical properties associated with amorphous semiconductors. This will be achieved through the development of an empirical model for the distributions of valence band and conduction band electronic states, the

distributions of defect states being explicitly included in this model, and the determination of the corresponding JDOS function from this model. Given that the JDOS function is directly related to the imaginary part of the dielectric function, $\epsilon_2(E)$, and the spectral dependence of the optical absorption coefficient, $\alpha(E)$, this will allow one to relate the underlying distributions of electronic states with the corresponding optical response. Through a fit with the results of experiment, the underlying form of the distribution of electronic states may thus be determined.

In this chapter, the background required for this work is provided. The analysis begins with an expression for the spectral dependence of the imaginary part of the dielectric function in terms of the energy levels of the individual states associated with the valence and conduction bands. Then, a number of simplifying assumptions are introduced, within the framework of a dipole matrix element based formalism, a relationship between the imaginary part of the dielectric function and the density of states (DOS) functions being developed. A free electron DOS model is then presented. Finally, a brief review of the development of a number of empirical DOS models, appropriate for the treatment of amorphous semiconductors, is then provided.

This chapter is organized in following manner. In Section 2.2, an expression for the spectral dependence of the imaginary part of the dielectric

function, $\epsilon_2(E)$, is presented. This expression is given in terms of the valence and conduction band electronic state energy levels and the corresponding optical transition matrix elements. Then, three simplifying assumptions are introduced in Section 2.3, these assumptions allowing one to simplify the expression for the imaginary part of the dielectric function for the specific case of a-Si. In Section 2.4, a dipole matrix element based formalism is introduced in order to develop a relationship between the imaginary part of the dielectric function, $\epsilon_2(E)$, and the valence and conduction band DOS functions. An aggregate dipole matrix element arises as a byproduct of this particular formalism. Then, in Section 2.5, the free electron model, for the DOS functions, is introduced. Finally, in Section 2.6, a brief review on the development of models for the DOS functions associated with an amorphous semiconductor, is provided.

2.2 The imaginary part of the dielectric function

Optical transitions occur between the occupied valence band electronic states and the unoccupied conduction band electronic states. For a linear response, within the framework of a one-electron perspective, Jackson *et al.* [6] assert that the imaginary part of the dielectric function,

$$\epsilon_2(E) = \left(\frac{2\pi q\hbar}{m_e E}\right)^2 \frac{2}{\mathcal{V}} \sum_{v,c} |\vec{\boldsymbol{\eta}}.\vec{\boldsymbol{\mathcal{P}}}_{v,c}|^2 \delta(E_c - E_v - E), \tag{2.1}$$

where q denotes the electron charge, m_e is the free electron mass, $\mathcal{V}$ is the illuminated volume, $\vec{\boldsymbol{\eta}}$ is the polarization vector of the incident light, and E is the incident photon energy, E_v and E_c corresponding to representative valence band (initial state) and conduction band (final state) electronic states, respectively. The matrix element, $\vec{\boldsymbol{\mathcal{P}}}_{v,c}$, which is defined as $\vec{\boldsymbol{\mathcal{P}}}_{v,c} = \langle c \,|\vec{\boldsymbol{\mathcal{P}}}|\, v\rangle$, where $\vec{\boldsymbol{\mathcal{P}}}$ denotes the momentum operator, $|v\rangle$ is a representative valence band electronic state, and $|c\rangle$ is a representative conduction band electronic state, couples the electronic states between which an optical transition may occur, i.e., it determines the probability of an optical transition between such states. The summation in Eq. (2.1), performed within the framework of the aforementioned one-electron perspective, is performed over all of the occupied valence band and unoccupied conduction band electronic states.

2.3 Simplifying assumptions

The imaginary part of the dielectric function, $\epsilon_2(E)$, is expressed in Eq. (2.1) in terms of the valence band and conduction band energy levels, E_v and E_c, respectively, and the magnitude of the corresponding momentum matrix elements, $\vec{\boldsymbol{\mathcal{P}}}_{v,c}$. This expression is generally applicable, for both the

amorphous and crystalline semiconductor cases. For the specific case of an amorphous semiconductor, however, the imaginary part of the dielectric function, $\epsilon_2(E)$, may be related to the distribution of valence band and conduction band electronic states by invoking three critical assumptions: (1) the incident light is unpolarized, (2) the momentum conservation rules are relaxed, and (3) zero-temperature statistics apply. The consequence of each of these assumptions is discussed subsequently.

The use of unpolarized light simplifies Eq. (2.1). Assuming random polarization, the directional average of $|\vec{\eta}.\vec{\boldsymbol{\mathcal{P}}}_{v,c}|^2$ reduces to $\frac{1}{3}|\mathcal{P}_{v,c}|^2$, where $|\mathcal{P}_{v,c}|$ denotes the amplitude of the momentum matrix element. As a consequence, Eq. (2.1) reduces to

$$\epsilon_2(E) = \left(\frac{2\pi q\hbar}{m_e E}\right)^2 \frac{2}{3\mathcal{V}} \sum_{v,c} |\mathcal{P}_{v,c}|^2 \delta(E_c - E_v - E). \tag{2.2}$$

Within a crystalline semiconductor, momentum is conserved during an optical transition. In contrast, for the case of an amorphous semiconductor, the momentum conservation rules are relaxed. That is, from every occupied valence band electronic state, optical transitions are possible to every unoccupied conduction band electronic state, assuming that the spin states are coincident, Jackson *et al.* [6] asserting that spin-flips are not allowed during such an optical transition. As a consequence, the momentum matrix element, $|\mathcal{P}_{v,c}|$, is constant for all possible optical transitions in the amor-

phous case, while it may vary greatly for the crystalline semiconductor case. This relaxation in the momentum conservation rules allows for a further simplification in the subsequent analysis.

In order to understand how a relaxation in the conservation rules impacts upon the allowed optical transitions, consider the case of N silicon atoms. For the case of c-Si, from every occupied valence band electronic states, there are four possible optical transitions, while for the case of a-Si, $2N$ optical transitions are possible, as the momentum conservation rules are relaxed. The number of possible optical transitions, for both cases, are stylistically depicted in Figure 2.1.

The third simplifying assumption is that of zero-temperature occupation statistics. The occupancy function, i.e., the probability of a given electronic state being occupied, also referred to as the Fermi-Dirac distribution function [10], may be expressed as

$$f(E) = \frac{1}{1 + \exp(\frac{E - E_F}{k_b T})}. \tag{2.3}$$

The dependence of this occupancy function on temperature is depicted in Figure 2.2, three different temperature levels being considered. Here, E_F denotes the Fermi energy level, k_b is the Boltzmann constant, and T is the temperature. It is noted that at absolute zero-temperature, i.e., at $T = 0\ K$, this function behaves as a step-function, where the step is at the

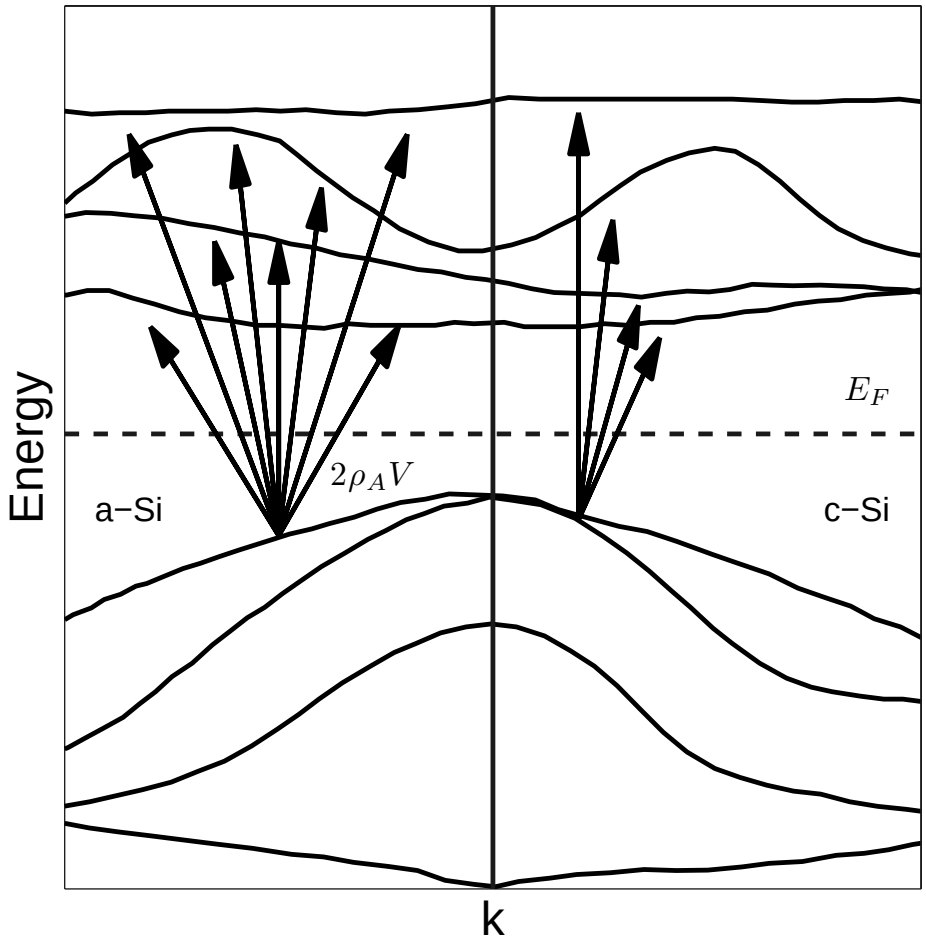

Figure 2.1: The number of possible optical transitions within c-Si and a-Si. This figure is after Jackson *et al.* [6].

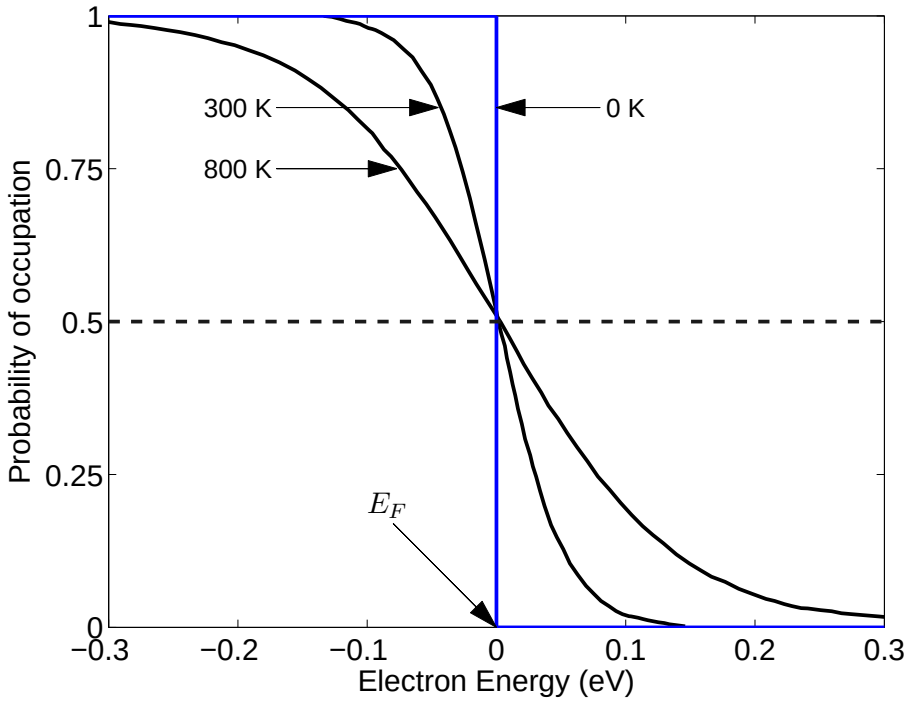

Figure 2.2: The occupancy function, $f(E)$, as a function of the energy, E, for three different temperature selections. The reference energy level, i.e., the Fermi energy level, E_F, is set to 0 eV for the purposes of all of the plots.

Fermi energy level itself, i.e., at $E = E_F$. For the case of semiconductors, at $T = 0\ K$, the occupancy probability is unity for the valence band states and zero for the conduction band states, i.e., all the valence band electronic states are fully occupied and all the conduction band electronic states are fully unoccupied. This assumption simplifies the subsequent analysis.

2.4 The relationship between the optical functions and the DOS functions

In order to smooth the variations in $|\mathcal{P}_{v,c}|$ that occur from optical transition to optical transition, researchers have found it useful to introduce an aggregate matrix element, $\mathcal{P}^2(E)$, which corresponds to the average value of $|\mathcal{P}^2_{v,c}|$ over all of the optical transitions that occur at energy E. It was often simply assumed that $\mathcal{P}^2(E)$ is independent of the photon energy, E. Cody *et al.* [7] attempted to validate this constant momentum matrix element assumption with some experimental data. For this purpose, they prepared a large number of a-Si:H samples of different thicknesses. They observed that although the spectral dependence of the optical functions can be satisfactorily explained assuming a constant $\mathcal{P}^2(E)$, the fit with experiment considerably improves when one instead assumes a constant dipole matrix

element. Moreover, a thickness dependence artifact, observed in the experimental results of Cody *et al.* [7], disappears when one adopts the constant dipole matrix element assumption. Based on these experimental observations of Cody *et al.* [7], Jackson *et al.* [6] casts Eq. (2.1) in terms of the dipole-matrix elements rather than in terms of the momentum-matrix elements. In particular, from the commutator relations, Jackson *et al.* [6] find that

$$\sum_{v,c} |\vec{\boldsymbol{\eta}}.\vec{\mathbf{P}}_{v,c}|^2 \delta(E_c - E_v - E) = \left(\frac{m_e E}{\hbar^2}\right)^2 \sum_{v,c} |\vec{\boldsymbol{\eta}}.\vec{\boldsymbol{\mathcal{R}}}_{v,c}|^2 \delta(E_c - E_v - E), \quad (2.4)$$

where $\vec{\boldsymbol{\mathcal{R}}}_{v,c} = \langle c|\vec{\boldsymbol{\mathcal{R}}}|v\rangle$ is the dipole-matrix element and $\vec{\boldsymbol{\mathcal{R}}}$ is the dipole operator. As was mentioned previously, for the case of a-Si, if the incident light is unpolarized, the directional average of $|\vec{\boldsymbol{\eta}}.\vec{\boldsymbol{\mathcal{R}}}_{v,c}|^2$ reduces to $\frac{1}{3}|\mathcal{R}_{v,c}|^2$, where $|\mathcal{R}_{v,c}|$ denotes the amplitude of the dipole matrix element. As a consequence

$$\begin{aligned} \epsilon_2(E) &= (2\pi q)^2 \frac{2}{3\mathcal{V}} \sum_{v,c} |\mathcal{R}_{v,c}|^2 \delta(E_c - E_v - E), \\ &= (2\pi q)^2 \frac{2}{3\mathcal{V}} [\mathcal{R}'(E)]^2 \sum_{v,c} \delta(E_c - E_v - E). \end{aligned} \quad (2.5)$$

So far, the derived expression, i.e., Eq. (2.5), is applicable for both c-Si and a-Si. In order to facilitate a direct comparison between the matrix elements associated with these two different materials, the dipole matrix elements should be normalized by a factor that is proportional to the ra-

tio between the numbers of allowed optical transitions, corresponding to each material, i.e., $\frac{2N}{4}$, so that the overall 'optical strength' remains constant. Letting ρ_A denote the atomic density of the Si atoms within a-Si, this normalization factor becomes $\frac{2\rho_A\mathcal{V}}{4}$. Following this assumption, Jackson *et al.* [6] introduced a normalized average dipole matrix element

$$\mathcal{R}^2(E) = \frac{\rho_A\mathcal{V}}{2}[\mathcal{R}'(E)]^2, \tag{2.6}$$

where $[\mathcal{R}'(E)]^2$ is the dipole matrix element squared averaged over all optical transitions separated by the energy E. This matrix element may be defined as

$$[\mathcal{R}'(E)]^2 \equiv \frac{\sum\limits_{v,c}\delta(E_c - E_v - E)|\mathcal{R}_{v,c}|^2}{\sum\limits_{v,c}\delta(E_c - E_v - E)}. \tag{2.7}$$

Using the relationship defined in Eq. (2.6), it is noted that Eq. (2.5) can be represented as

$$\epsilon_2(E) = (2\pi q)^2\frac{2}{3\mathcal{V}}\left(\frac{2}{\rho_A\mathcal{V}}\right)\mathcal{R}^2(E)\sum_{v,c}\delta(E_c - E_v - E). \tag{2.8}$$

The last term, $\sum\limits_{v,c}\delta(E_c - E_v - E)$, in Eq. (2.8) provides information on the number of possible optical transitions between the occupied valence band and the unoccupied conduction band states, separated by energy E. Defining the JDOS function,

$$J(E) \equiv \frac{4}{\mathcal{V}}\sum_{v,c}\delta(E_c - E_v - E), \tag{2.9}$$

from Eqs. (2.8) and (2.9), one can thus conclude that

$$\epsilon_2(E) = \frac{(2\pi q)^2}{3\rho_A}\mathcal{R}^2(E)J(E). \tag{2.10}$$

The valence band DOS function, $N_v(E)$, where $N_v(E)\Delta E$ represents the number of one electron valence band states, between energies $[E, E + \Delta E]$, per unit volume, may be expressed as

$$N_v(E) = \frac{2}{\mathcal{V}}\sum_v \delta(E - E_v), \tag{2.11}$$

the sum being taken over all of the valence band single-spin electronic states divided by the volume, the factor of 2 representing the fact that each electronic state considered is single-spin, i.e., there are two possible spins. Similarly, one can define the conduction band DOS function, $N_c(E)$, where $N_c(E)\Delta E$ represents the number of one electron conduction band states, between energies $[E, E + \Delta E]$, per unit volume, it can be expressed as

$$N_c(E) = \frac{2}{\mathcal{V}}\sum_c \delta(E - E_c). \tag{2.12}$$

As before, in Eq. (2.12), the factor 2 represents the fact that each electronic state is single-spin, i.e., there are two possible spins.

For zero-temperature statistics, i.e., assuming that all of the valence band electronic states are fully occupied and that all of the conduction band electronic states are completely unoccupied, the JDOS function may be expressed as an integral over the valence band and the conduction band

DOS functions. That is,

$$J(E) = \int_{-\infty}^{\infty} N_v(\xi) N_c(E+\xi) d\xi. \tag{2.13}$$

For the specific case of a-Si, given that the density of Si atoms within a-Si is around 4.4×10^{22} cm^{-3} [8], it can be seen that Eq. (2.10) may be expressed as

$$\epsilon_2(E) = 4.3 \times 10^{-45} \mathcal{R}^2(E) J(E), \tag{2.14}$$

where $\mathcal{R}^2(E)$ is in unit of Å^2 and $J(E)$ is in the unit of cm^{-6}eV^{-1} [6].

The spectral dependence of the optical absorption coefficient can be determined [4] by noting that,

$$\alpha(E) = \frac{E}{n(E) c \hbar} \epsilon_2(E), \tag{2.15}$$

where $n(E)$ denotes the spectral dependence of the index of refraction, c represents the speed of the light in vacuum, and $\hbar$ is the reduced Plank's constant. The spectral dependence of the refractive index, $n(E)$, is determined by fitting a tenth-order polynomial to the experimental results of Klazes *et al.* [9]; the experimental data considered for determining $n(E)$ corresponds to that presented in Figure 4 of Klazes *et al.* [9]; this technique was used previously by Thevaril [4].

2.5 A free electron model for the DOS function

Consider a three-dimensional cubic box, of dimensions $L \times L \times L$, within which an electron is confined, as depicted in Figure 2.3. According to quantum mechanics, for steady-state conditions, the wavefunctions associated with this confined electron can be determined through the solution of the steady-state, three-dimensional Schrödinger's equation [10], i.e.,

$$\frac{\partial^2 \Psi}{\partial x^2} + \frac{\partial^2 \Psi}{\partial y^2} + \frac{\partial^2 \Psi}{\partial z^2} + \frac{2m_e}{\hbar^2}(E - V)\Psi(x, y, z) = 0, \tag{2.16}$$

where m_e, E, and V denote the free electron mass, the electron energy, and the potential energy, respectively. If it is assumed that the electron is totally free within the cubic box itself, i.e., V=0 for $0 \leq x \leq L$, $0 \leq y \leq L$, and $0 \leq z \leq L$, and if the potential outside the box is infinite, then it can be shown that,

$$\Psi_{n_x n_y n_z}(x, y, z) = \left(\frac{2}{L}\right)^{2/3} \sin\left(\frac{n_x \pi x}{L}\right) \sin\left(\frac{n_y \pi y}{L}\right) \sin\left(\frac{n_z \pi z}{L}\right), \tag{2.17}$$

where n_x, n_y, and n_z are positive integers associated with the electron's motion in the x, y, and z directions, respectively, denoting the corresponding quantum numbers. The energy of the corresponding electronic states may be found by substituting this solution for the wavefunction, i.e., Eq. (2.17), back into Schrödinger's equation. It may thus be shown that

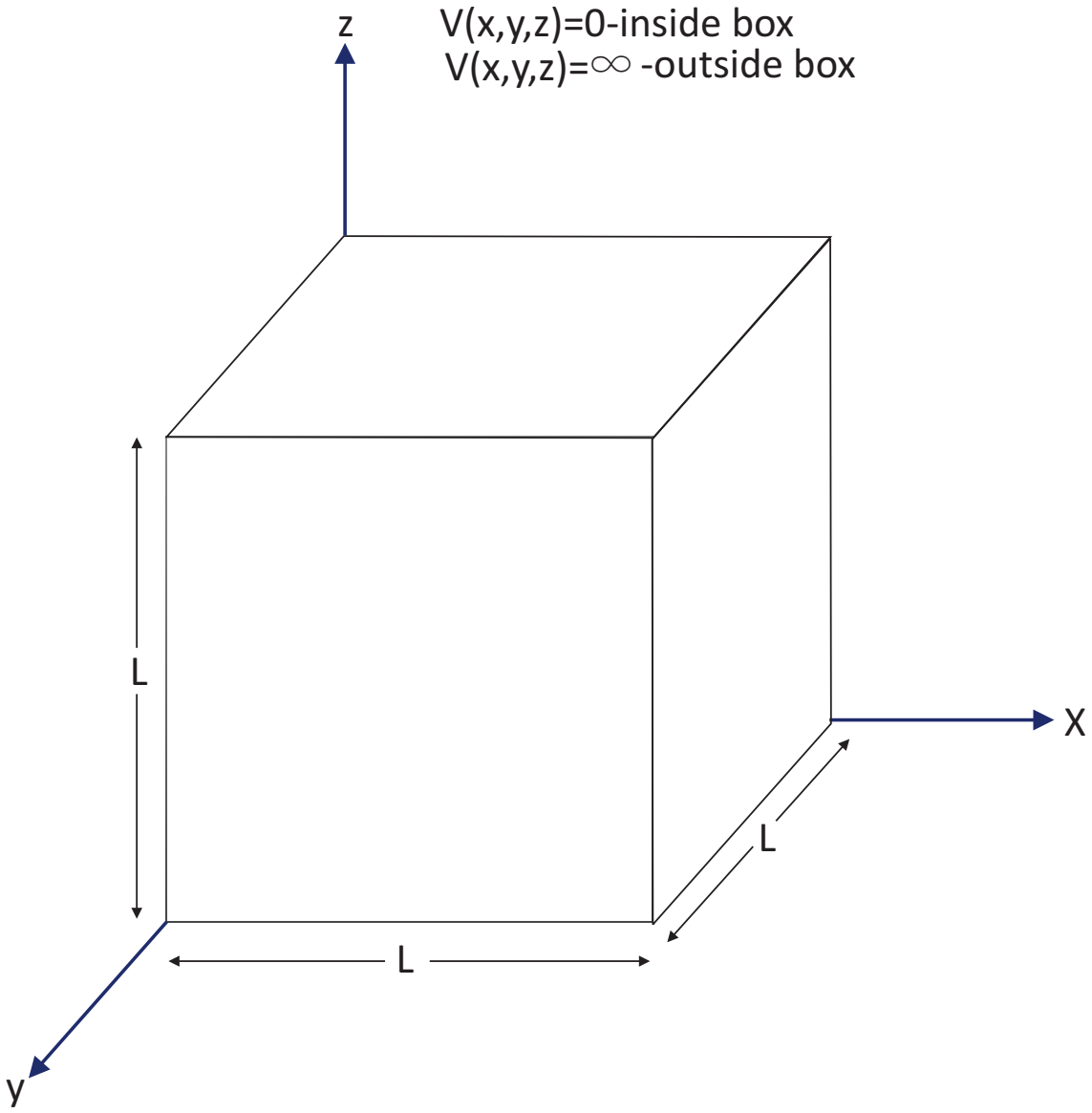

Figure 2.3: An electron confined within a cubic volume, of dimensions $L \times L \times L$, surrounded by infinite potentials barriers.

$$E_{n_x n_y n_z} = \frac{\hbar^2}{2m_e}\left[\left(\frac{n_x\pi}{L}\right)^2 + \left(\frac{n_y\pi}{L}\right)^2 + \left(\frac{n_z\pi}{L}\right)^2\right], \tag{2.18}$$

where $E_{n_x n_y n_z}$ represents the energy level corresponding to the wavefunction, $\Psi_{n_x n_y n_z}(x, y, z)$. It is clear that these energy levels depend on three quantum numbers, i.e., n_x, n_y, and n_z. In the continuum limit, i.e., for large values of energy, E, the associated DOS function may be expressed as

$$N(E) = \begin{cases} \sqrt{2}\ \frac{m_e^{3/2}}{\pi^2\hbar^3}\sqrt{E},\ E \geq 0 \\ \\ 0,\ E < 0 \end{cases} . \tag{2.19}$$

It is seen that this DOS function has no dependence on the cubic dimensions, i.e., L, in of itself. That is, when $L \to \infty$, i.e., when the confined electron becomes totally free, the DOS function still remains the same. This square-root DOS function, often referred to as the free-electron DOS model, provides the basis for the subsequent analysis.

2.6 A review of models for the density of state functions

The nature of the disorder that is present within a-Si has been the focus of investigation for many years. It is widely assumed that disorder plays an important role in shaping the optical response of an amorphous semiconductor, i.e., it produces a distribution of electronic states that encroaches

into the otherwise empty gap region. The distribution of electronic states that encroach into the gap region are generally referred to as tail states. In order to provide a theoretical basis for understanding the nature of the optical absorption spectrum associated with an amorphous semiconductor, the DOS functions associated with these materials must be known. For many years, the exact role that disorder plays in influencing the form of the DOS functions has been under investigation. A brief review of the DOS models, that have been proposed in the past, is provided next.

Based on the free-electron DOS model, in 1966, Tauc *et al.* [11] proposed an empirical DOS model for both the valence band and conduction band DOS functions. In particular, Tauc *et al.* [11] assumes that

$$N_v(E) = \begin{cases} N_{vo}\sqrt{E_v - E}, & E \leq E_v \\ 0, & E > E_v \end{cases}, \tag{2.20}$$

and that

$$N_c(E) = \begin{cases} N_{co}\sqrt{E - E_c}, & E \geq E_c \\ 0, & E < E_c \end{cases}, \tag{2.21}$$

where N_{vo} and N_{co} denote the valence band and conduction band DOS prefactors, respectively, E_v and E_c represent the valence band and conduction band band edges, and E is the energy. The resultant DOS functions, for the nominal selections of DOS modeling parameters tabulated in Table 2.1, are

depicted in Figure 2.4. This model forms the basis for the determination of the optical gap associated with an amorphous semiconductor.

In 1981, an improved model of Tauc *et al.* [11] was devised by Chen *et al.* [12], in which an exponential distribution of tail states is splined onto a square-root distribution of valence band states; Chen *et al.* [12] only assumed exponential tail states for the valence band DOS function, $N_v(E)$, the conduction band DOS function, $N_c(E)$, being exactly same as that of Tauc *et al.* [11]. Chen *et al.* [12] thus assume that

$$N_v\left(E\right) = \begin{cases} N_{vo}\sqrt{E_v - E},\ E \leq E_v \\ \\ N_{vo}^{*}\exp\left(\frac{E_v - E}{\gamma_v}\right),\ E > E_v \end{cases}, \tag{2.22}$$

and that

$$N_c\left(E\right) = \begin{cases} 0,\ E < E_c \\ \\ N_{co}\sqrt{E - E_c},\ E \geq E_c \end{cases}, \tag{2.23}$$

where N_{vo}^{*} represents the valence band tail prefactor and γ_v denotes the valence band tail breadth. All other parameters are the same as defined earlier. The resultant DOS functions, for the nominal selections of the DOS modeling parameters tabulated in Table 2.1, are depicted in Figure 2.5.

There is general consensus that the optical properties of a semiconductor are greatly influenced by both the valence band and the conduction band tails. Following Chen *et al.* [12], Redfield [13] proposed a new model where

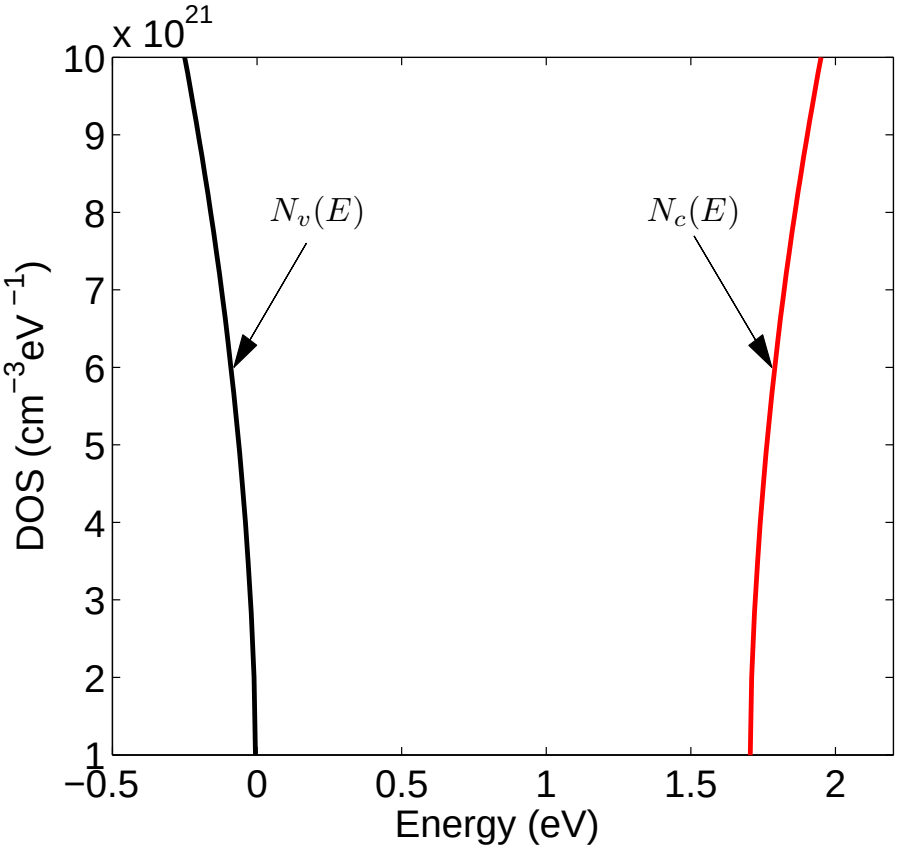

Figure 2.4: The valence band and conduction band DOS functions, plotted as a function of energy, E, determined using the DOS model of Tauc *et al.* [11].

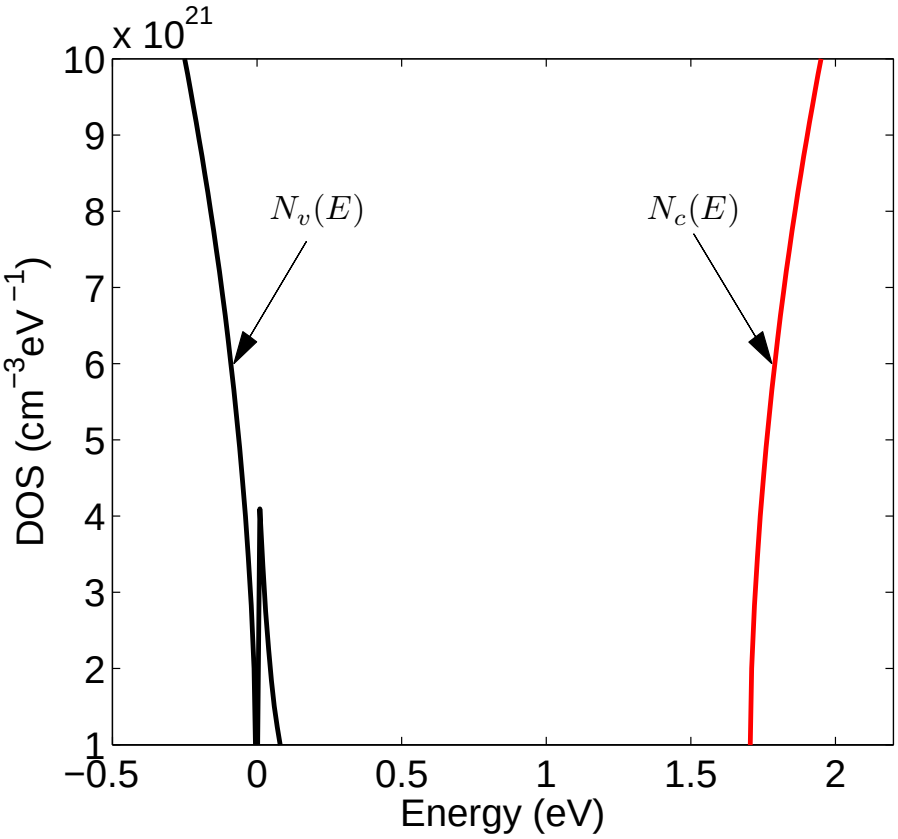

Figure 2.5: The valence band and conduction band DOS functions, plotted as a function of energy, E, determined using the DOS model of Chen *et al.* [12].

Table 2.1: The nominal DOS modeling parameters corresponding to a-Si. These parameter selections, employed for the empirical DOS models described in this section, are from Thevaril [4].

Parameter (unit)	Tauc *et al.* [11]	Chen *et al.* [12]	Redfield [13]	Cody [14]	O'Leary *et al.* [15]
N_{vo} ($\mathrm{cm}^{-3}\mathrm{eV}^{-3/2}$)	2×10^{22}	2×10^{22}	-	2×10^{22}	2×10^{22}
N_{co} ($\mathrm{cm}^{-3}\mathrm{eV}^{-3/2}$)	2×10^{22}	2×10^{22}	-	2×10^{22}	2×10^{22}
N^*_{vo} ($\mathrm{cm}^{-3}\mathrm{eV}^{-3/2}$)	-	5×10^{21}	5×10^{21}	-	-
N^*_{co} ($\mathrm{cm}^{-3}\mathrm{eV}^{-3/2}$)	-	-	5×10^{21}	-	-
E_v (eV)	0	0	0	0	0
E_c (eV)	1.7	1.7	1.7	1.7	1.7
$E_v - E_{v_\mathrm{T}}$ (meV)	-	-	-	-	25
$E_{c_\mathrm{T}} - E_c$ (meV)	-	-	-	-	13.5
γ_v (meV)	-	50	50	50	50
γ_c (meV)	-	-	27	-	27

the conduction band tail states are also included. However, Redfield [13] assumes constant distributions of valence band and conduction band band states. That is, Redfield [13] assumes that

$$N_v(E) = \begin{cases} N^*_{vo}, & E \leq E_v \\ N^*_{vo} \exp\left(\frac{E_v - E}{\gamma_v}\right), & E > E_v \end{cases}, \tag{2.24}$$

and that

$$N_c(E) = \begin{cases} N^*_{co}, & E \geq E_c \\ N^*_{co} \exp\left(\frac{E - E_c}{\gamma_c}\right), & E < E_c \end{cases}, \tag{2.25}$$

where N^*_{co} represents the conduction band tail prefactor and γ_c denotes the conduction band tail breadth. All other parameters are the same as defined earlier. The resultant DOS functions, for the nominal selections of the DOS

modeling parameters tabulated in Table 2.1, are depicted in Figure 2.6.

Later on, a further improved model was developed, based on the models of Chen *et al.* [12] and Redfield [13]. In 1984, Cody [14] proposed a new model, where it is assumed that the exponential tail states occur below the square-root band band edge, E_v, differing from Chen *et al.* [12] in the sense that Chen *et al.* [12] assume an exponential band tail splined onto a terminated square-root band state. That is, Cody [14] asserts that

$$N_v(E) = \begin{cases} N_{vo}\sqrt{E_v - E},\ E \leq E_v - \frac{3}{2}\gamma_v \\ N_{vo}\sqrt{\frac{3}{2}\gamma_v}\exp\left(-\frac{3}{2}\right)\exp\left(\frac{E_v - E}{\gamma_v}\right),\ E > E_v - \frac{3}{2}\gamma_v \end{cases}, \quad (2.26)$$

and that

$$N_c(E) = \begin{cases} N_{co}\sqrt{E - E_c},\ E \geq E_c \\ 0,\ E < E_c \end{cases}, \quad (2.27)$$

where all the DOS modeling parameters are the same as defined earlier. The resultant DOS functions, for the nominal selections of the DOS modeling parameters tabulated in Table 2.1, are depicted in Figure 2.7.

The empirical DOS model of Cody [14] was further improved by O'Leary *et al.* [15]. In 1997, they proposed a new model, where it was assumed: (1) square-root distributions of band states and exponential distributions of tail states, for the valence band and conduction band, and (2) the valence band and conduction band DOS functions, $N_v(E)$ and $N_c(E)$, and their

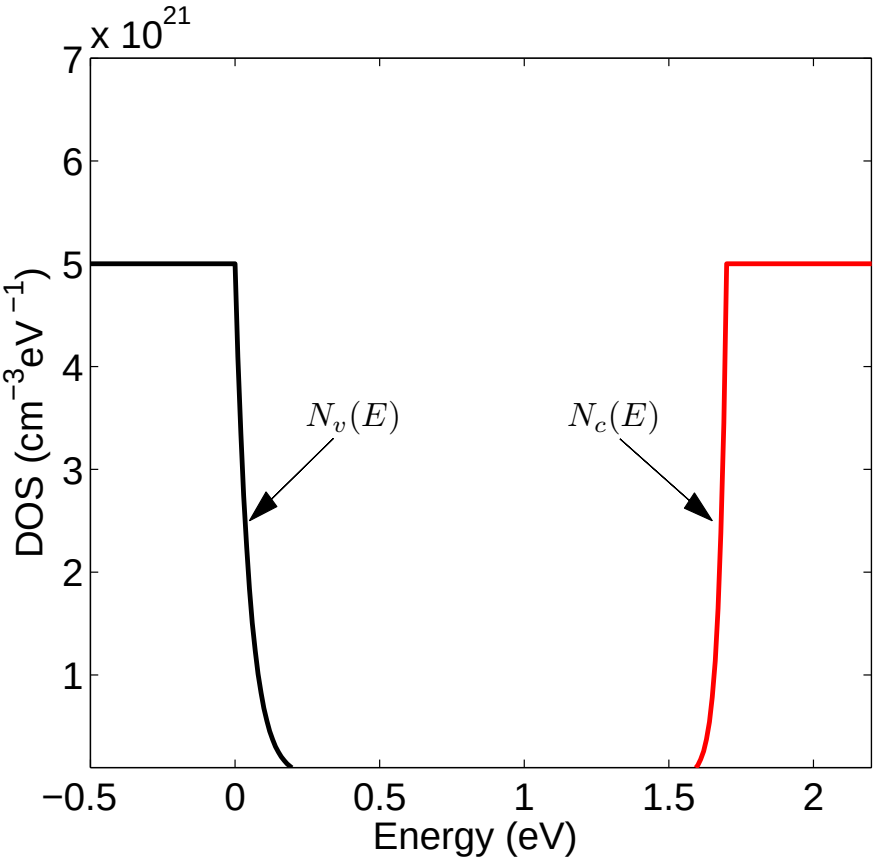

Figure 2.6: The valence band and conduction band DOS functions, plotted as a function of energy, E, determined using the DOS model of Redfield [13].

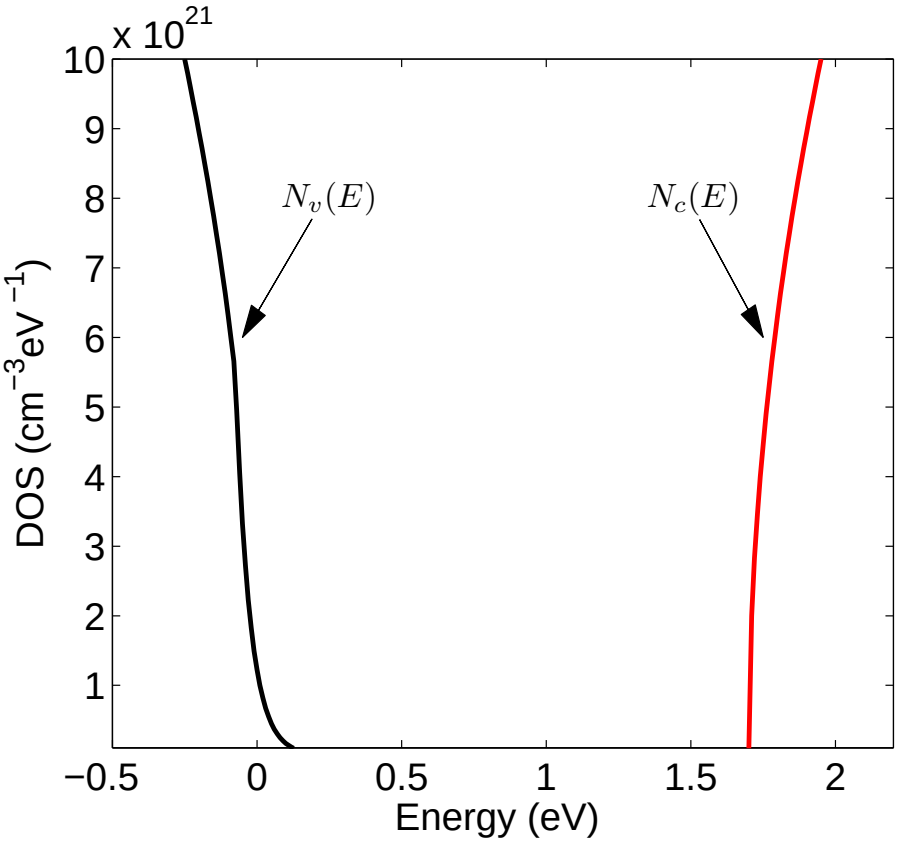

Figure 2.7: The valence band and conduction band DOS functions, plotted as a function of energy, E, determined using the DOS model of Cody [14].

derivatives, are continuous at the critical energies at which the square-root distributions and exponential distributions interface. That is, O'Leary *et al.* [15] assert that

$$N_v(E) = N_{vo} \begin{cases} \sqrt{E_v - E}, & E \leq E_v - \frac{\gamma_v}{2} \\ \sqrt{\frac{\gamma_v}{2}} \exp\left(-\frac{1}{2}\right) \exp\left(\frac{E_v - E}{\gamma_v}\right), & E > E_v - \frac{\gamma_v}{2} \end{cases}, \quad (2.28)$$

and that

$$N_c(E) = N_{co} \begin{cases} \sqrt{E - E_c}, & E \geq E_c + \frac{\gamma_c}{2} \\ \sqrt{\frac{\gamma_c}{2}} \exp\left(-\frac{1}{2}\right) \exp\left(\frac{E - E_c}{\gamma_c}\right), & E < E_c + \frac{\gamma_c}{2} \end{cases}, \quad (2.29)$$

where all of the DOS modeling parameters are the same as defined earlier. The resultant DOS functions, for the nominal selections of the DOS modeling parameters tabulated in Table 2.1, are depicted in Figure 2.8.

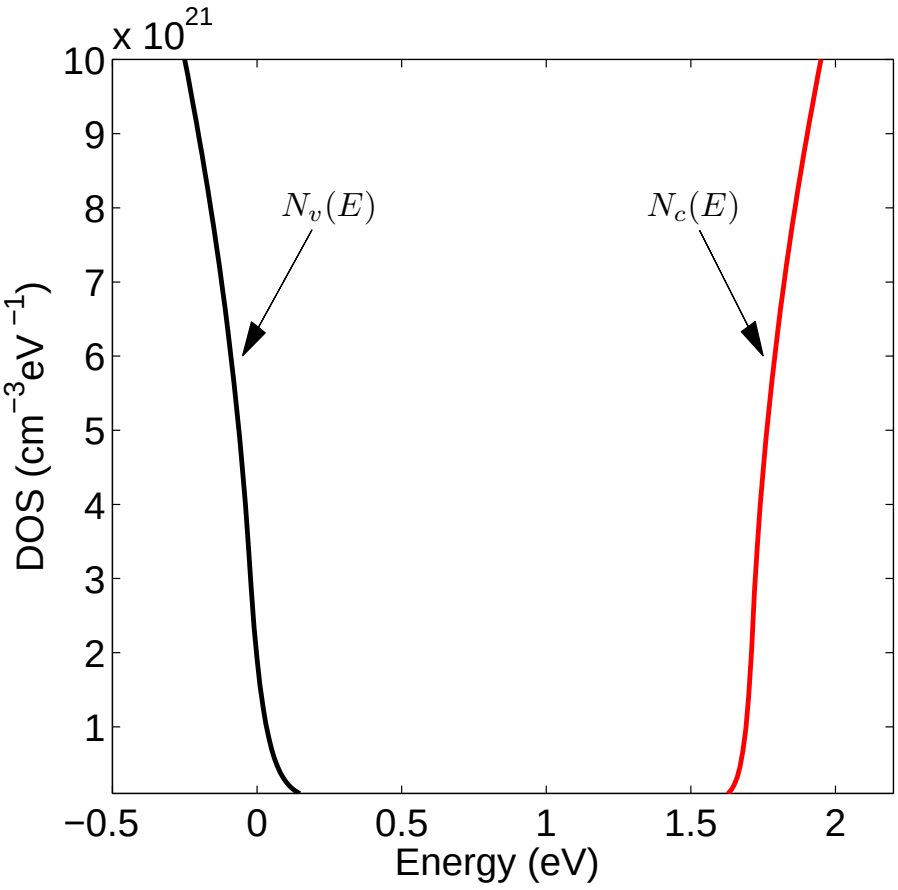

Figure 2.8: The valence band and conduction band DOS functions, plotted as a function of energy, E, determined using the DOS model of O'Leary *et al.* [15].

Chapter 3

DOS and JDOS analysis:

Single defect band model

3.1 DOS and JDOS analysis

It has already been established that defects play an important role in shaping the optical response of a semiconductor. Defects also influence the corresponding electronic properties. Understanding how defects are distributed within the energy gap of a semiconductor is of critical importance to understanding how a material responds to light and in evaluating how such a response impacts upon the performance of a given device. Defect states will produce a distinctive broadening of the JDOS function associated with an amorphous semiconductor in the sub-gap region and this will shape the form of the JDOS function, $J(E)$, the imaginary part of the dielectric function, $\epsilon_2(E)$, and the optical absorption spectrum, $\alpha(E)$.

In this chapter, two empirical models for the valence band and conduction band DOS functions, $N_v(E)$ and $N_c(E)$, are presented, defect states being included in these models. Assuming square-root distributions of band states and exponential distributions of tail states, the distribution of defect valence band and conduction band states will be treated through the introduction of an additional exponential tail that is broader than that associated with the intrinsic tail. The contributions to the JDOS function, attributable to the various possible types of optical transitions, are then evaluated.

This chapter is organized in the following manner. In Section 3.2, a detailed conduction band defect model is presented. Then, in Section 3.3, a detailed valence band defect model is presented.

3.2 Conduction band defect model

The analysis is performed within the framework of a general empirical model for the DOS functions, $N_v(E)$ and $N_c(E)$, that captures the basic expected features. For the case of a-Si:H, in the absence of defect states, there is a general consensus that $N_v(E)$ and $N_c(E)$ exhibit square-root functional dependencies in the band regions and exponential functional dependencies in the tail regions. Following O'Leary [16], one can thus set

$$N_v\left(E\right) = N_{vo}\begin{cases} \sqrt{E_v - E_{v_{\mathrm{T}}}}\ \exp\left(\frac{E_{v_{\mathrm{T}}} - E_v}{\gamma_v}\right)\exp\left(\frac{E_v - E}{\gamma_v}\right) & E > E_{v_{\mathrm{T}}} \\ \sqrt{E_v - E}, & E \leq E_{v_{\mathrm{T}}} \end{cases}, \tag{3.1}$$

and

$$N_c\left(E\right) = N_{co}\begin{cases} \sqrt{E - E_c}, & E \geq E_{c_{\mathrm{T}}} \\ \sqrt{E_{c_{\mathrm{T}}} - E_c}\ \exp\left(\frac{E_c - E_{c_{\mathrm{T}}}}{\gamma_c}\right)\ \exp\left(\frac{E - E_c}{\gamma_c}\right), & E < E_{c_{\mathrm{T}}} \end{cases}, \tag{3.2}$$

where N_{vo} and N_{co} denote the valence band and conduction band DOS prefactors, respectively, E_v and E_c represent the valence band and conduction band band edges, γ_v and γ_c are the breadths of the valence band and conduction band tail distributions, $E_{v_{\mathrm{T}}}$ and $E_{c_{\mathrm{T}}}$ being the critical energies at which the exponential and square-root distributions interface; it should be noted that this model implicitly requires that $E_v - E_{v_{\mathrm{T}}} \geq 0$ and that $E_{c_{\mathrm{T}}} - E_c \geq 0$. From Eqs. (3.1) and (3.2), it is noted that $N_v(E)$ and $N_c(E)$ are continuous functions of energy.

To include the defect states, a new course of analysis is performed, similar to that employed by Shur and Hack [17]. In the model of Shur and Hack [17], the conduction band DOS below the band edge is comprised of two exponentially varying distributions, i.e., a narrow exponential distribution, corresponding to the intrinsic (without defects) tail states, and a broad

exponential distribution, corresponding to the defect states. A slightly different model, which captures the same spirit as that of Shur and Hack [17], but allows for an easier analysis, is employed here. This empirical model for the DOS functions captures the basic expected features of defect states. In particular, a distribution of conduction band defect (CBD) states is added onto the distribution of valence band band (VBB), valence band tail (VBT), conduction band band (CBB), and conduction band tail (CBT) states that are considered by Malik and O'Leary [18]. For this added distribution of defect states, optical transitions from the valence band band to the conduction band defect (VBB-CBD) states and from the valence band tail to the conduction band defect states (VBT-CBD), are to be considered, in addition to the VBB-CBB, VBB-CBT, VBT-VBB, and VBT-CBT optical transitions. The conduction band defect model is given by

$$N_v(E) = N_{vo} \begin{cases} \sqrt{E_v - E_{v_T}}\ \exp\left(\frac{E_{v_T} - E_v}{\gamma_v}\right) \exp\left(\frac{E_v - E}{\gamma_v}\right) & E > E_{v_T} \\ \sqrt{E_v - E}, & E \leq E_{v_T} \end{cases}, \tag{3.3}$$

and

$$N_c(E) = N_{co} \begin{cases} \sqrt{E - E_c}, & E \geq E_{c_\mathrm{T}} \\ \sqrt{E_{c_\mathrm{T}} - E_c}\ \exp\left(\frac{E_c - E_{c_\mathrm{T}}}{\gamma_c}\right)\ \exp\left(\frac{E - E_c}{\gamma_c}\right), & E_{c_\mathrm{D}} \leq E < E_{c_\mathrm{T}} \\ \sqrt{E_{c_\mathrm{T}} - E_c}\ \exp\left(\frac{E_c - E_{c_\mathrm{T}}}{\gamma_c}\right)\ \exp\left(\frac{E_{c_\mathrm{D}} - E_c}{\gamma_c}\right) & \\ \exp\left(\frac{E - E_{c_\mathrm{D}}}{\gamma_{c_\mathrm{D}}}\right), & E < E_{c_\mathrm{D}} \end{cases}, \tag{3.4}$$

where γ_{c_D} represents the breadth of the conduction band defect distribution and E_{c_D} is the critical energy at which the conduction band exponential and defect distributions interface. All other parameters are the same as defined earlier; as with the defect-free model, i.e., Eqs. (3.1) and (3.2). It is further assumed that $\gamma_{c_\mathrm{D}} \geq \gamma_c$ and that $E_{c_\mathrm{T}} > E_{c_\mathrm{D}}$ for the purposes of this analysis. The same nominal a-Si DOS modeling parameters, tabulated in Table 1 of Thevaril and O'Leary [19], are employed throughout the analysis. These DOS modeling parameters are tabulated in Table 3.1.

From Figure 3.1, it is clear that there are six different types of optical transitions that occur. These are: (1) VBB-CBB optical transitions, (2) VBB-CBT optical transitions, (3) VBB-CBD optical transitions, (4) VBT-CBB optical transitions, (5) VBT-CBT optical transitions, and (6) VBT-CBD optical transitions.

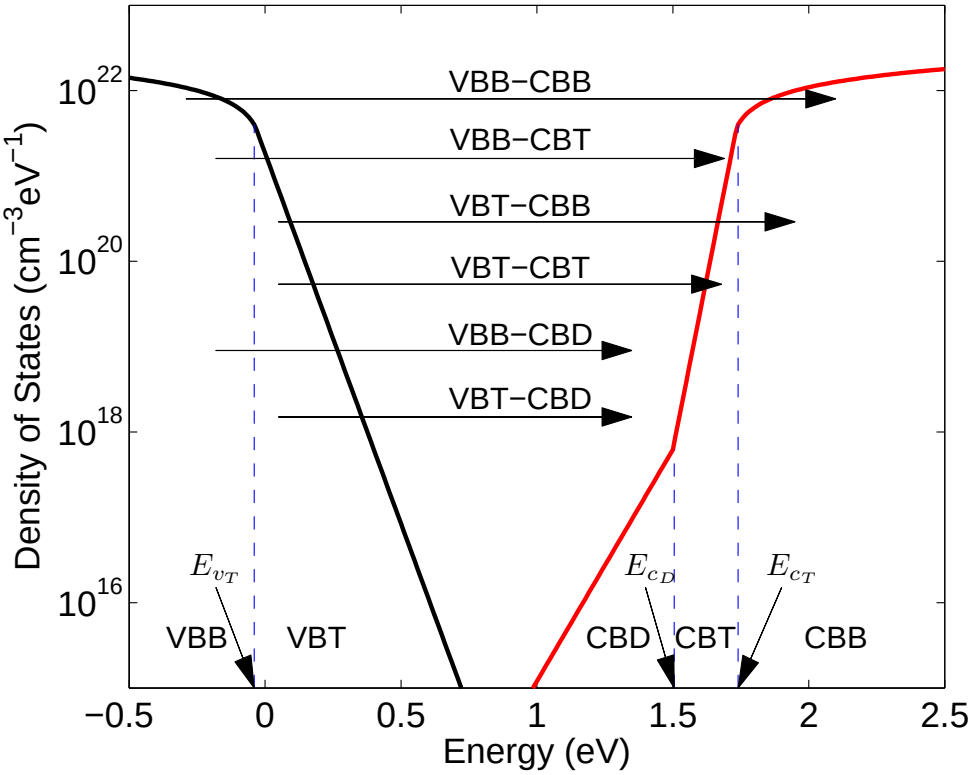

Figure 3.1: The valence band and conduction band DOS functions associated with a-Si. The critical energies in the DOS functions, i.e., $E_{v_{\mathrm{T}}}$, $E_{c_{\mathrm{T}}}$, and $E_{c_{\mathrm{D}}}$, are clearly marked with the dashed lines and the arrows. All of the possible optical transition are shown with the arrows. The DOS modeling parameters are as set in Table 3.1.

Table 3.1: The nominal a-Si DOS modeling parameter selections employed for the purposes of this analysis.

ParameterParameters(units)	Value
N_{vo} ($\mathrm{cm}^{-3}\mathrm{eV}^{-3/2}$)	2×10^{22}
N_{co} ($\mathrm{cm}^{-3}\mathrm{eV}^{-3/2}$)	2×10^{22}
E_v (eV)	0
E_c (eV)	1.7
γ_v (meV)	50
γ_c (meV)	27
$E_v - E_{v_\mathrm{T}}$ (meV)	35
$E_{c_\mathrm{T}} - E_c$ (meV)	35
γ_{c_D} (meV)	80
$E_c - E_{c_\mathrm{D}}$ (meV)	200

In order to understand how these different types of optical transitions contribute to overall optical response of this material, it is necessary to find the JDOS contributions corresponding to these six types of optical transitions. For this analysis, three different cases are considered, i.e.,

1. case 1 (subcase 1) $E_{v_\mathrm{T}} > E_{c_\mathrm{D}} - \hbar\omega$ and $E_{v_\mathrm{T}} > E_{c_\mathrm{T}} - \hbar\omega$,

2. case 1 (subcase 2) $E_{v_\mathrm{T}} > E_{c_\mathrm{D}} - \hbar\omega$ and $E_{v_\mathrm{T}} < E_{c_\mathrm{T}} - \hbar\omega$, and

3. case 2 $E_{v_\mathrm{T}} < E_{c_\mathrm{D}} - \hbar\omega$.

The first condition, $E_{v_\mathrm{T}} > E_{c_\mathrm{D}} - \hbar\omega$, implies that $\hbar\omega > E_{c_\mathrm{D}} - E_{v_\mathrm{T}}$, and $E_{v_\mathrm{T}} > E_{c_\mathrm{T}} - \hbar\omega$ implies that $\hbar\omega > E_{c_\mathrm{T}} - E_{v_\mathrm{T}}$. That is, it is assumed that $\hbar\omega > E_{c_\mathrm{T}} - E_{v_\mathrm{T}}$. The factors in the JDOS integrand are plotted as a function of E for this case in Figure 3.2. For the case of $\hbar\omega > E_{c_\mathrm{T}} - E_{v_\mathrm{T}}$, it is clear that VBB-CBB, VBB-CBT, VBB-CBD, and VBT-CBB optical

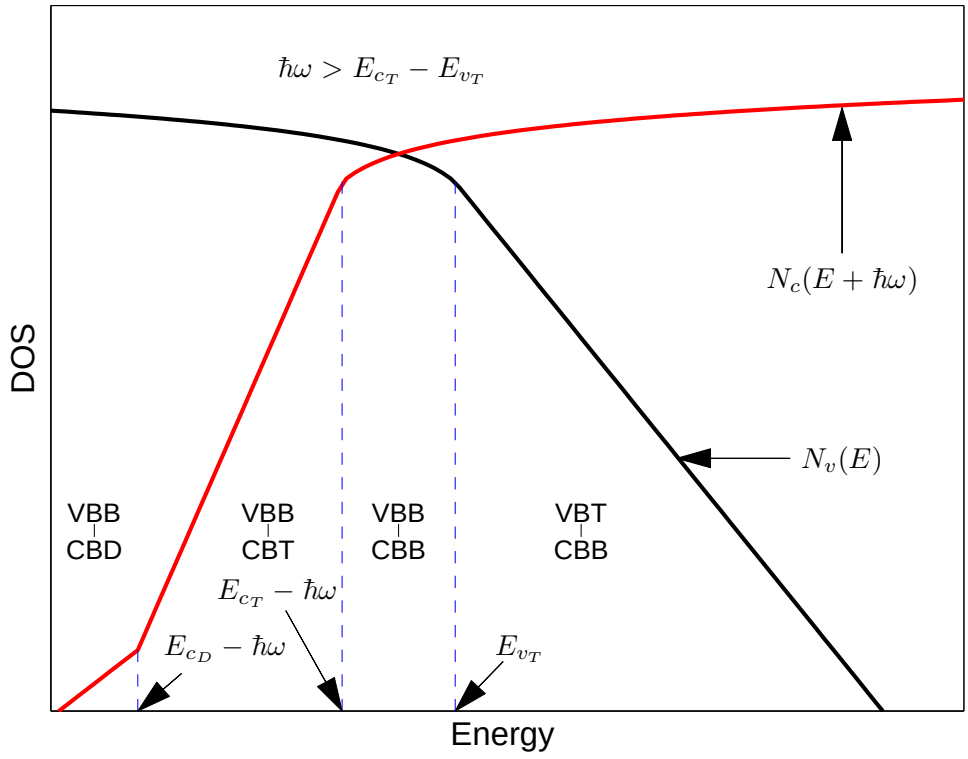

Figure 3.2: The factors in the JDOS integrand, $N_v(E)$ and $N_c(E+\hbar\omega)$, as a function of energy, E, for $\hbar\omega > E_{c_T} - E_{v_T}$. The DOS modeling parameters are as set in Table 3.1.

transitions contribute to the overall JDOS function. These contributions to the JDOS function are denoted $J_{\text{VBB-CBB}}(\hbar\omega)$, $J_{\text{VBB-CBT}}(\hbar\omega)$, $J_{\text{VBB-CBD}}(\hbar\omega)$, and $J_{\text{VBT-CBB}}(\hbar\omega)$, respectively, and correspond to the integrations of the JDOS integrand, $N_v(E)N_c(E+\hbar\omega)$, between energies $E_{c_\text{T}} - \hbar\omega$ and E_{v_T}, $E_{c_\text{D}} - \hbar\omega$ and $E_{c_\text{T}} - \hbar\omega$, $-\infty$ and $E_{c_\text{D}} - \hbar\omega$, and E_{v_T} and ∞. The JDOS contributions to the overall JDOS function, attributable to these different types of optical transitions, are enumerated below. That is,

$$J_{\text{VBB-CBB}}(\hbar\omega) = \int_{E_{c_\text{T}}-\hbar\omega}^{E_{v_\text{T}}} N_v(E)\, N_c(E+\hbar\omega)\; dE,$$

$$J_{\text{VBB-CBT}}(\hbar\omega) = \int_{E_{c_\text{D}}-\hbar\omega}^{E_{c_\text{T}}-\hbar\omega} N_v(E)\, N_c(E+\hbar\omega)\; dE,$$

$$J_{\text{VBB-CBD}}(\hbar\omega) = \int_{-\infty}^{E_{c_\text{D}}-\hbar\omega} N_v(E)\, N_c(E+\hbar\omega)\; dE,$$

$$J_{\text{VBT-CBB}}(\hbar\omega) = \int_{E_{v_\text{T}}}^{\infty} N_v(E)\, N_c(E+\hbar\omega)\; dE,$$

$$J_{\text{VBT-CBT}}(\hbar\omega) = 0,$$

and

$$J_{\text{VBT-CBD}}(\hbar\omega) = 0.$$

The second condition, $E_{v_\text{T}} > E_{c_\text{D}} - \hbar\omega$, implies that $\hbar\omega > E_{c_\text{D}} - E_{v_\text{T}}$. This suggests that $E_{v_\text{T}} < E_{c_\text{T}} - \hbar\omega$. That is, $E_{c_\text{T}} - E_{v_\text{T}} > \hbar\omega$ or $E_{c_\text{D}} - E_{v_\text{T}} < \hbar\omega < E_{c_\text{T}} - E_{v_\text{T}}$. The factors in the JDOS integrand are plotted as a function of E for this case in Figure 3.3. For the case of $E_{c_\text{D}} - E_{v_\text{T}} < \hbar\omega < E_{c_\text{T}} - E_{v_\text{T}}$, from Figure 3.3, it is clear that the contributions to the overall JDOS function, attributable solely to the VBB-CBT, VBB-CBD, VBT-CBT, and

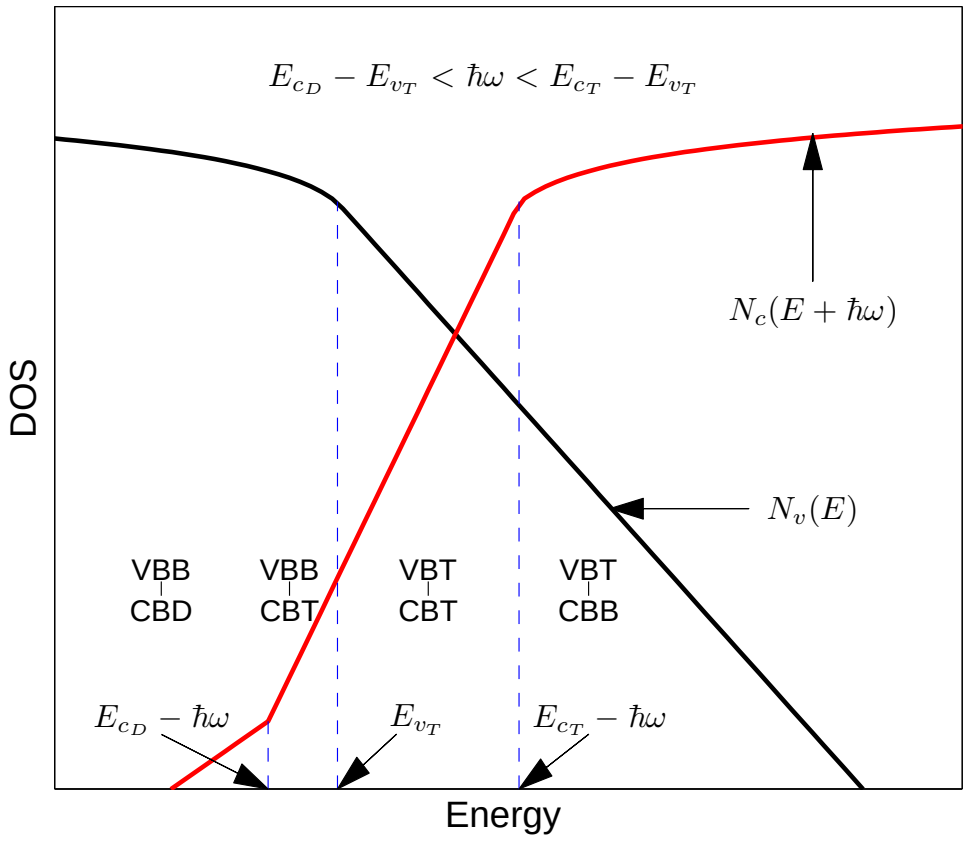

Figure 3.3: The factors in the JDOS integrand, $N_v(E)$ and $N_c(E+\hbar\omega)$, as a function of energy, E, for $E_{c_\mathrm{D}} - E_{v_\mathrm{T}} < \hbar\omega < E_{c_\mathrm{T}} - E_{v_\mathrm{T}}$. The DOS modeling parameters are as set in Table 3.1.

VBT-CBB optical transitions, i.e., $J_{\text{VBB-CBT}}(\hbar\omega)$, $J_{\text{VBB-CBD}}(\hbar\omega)$, $J_{\text{VBT-CBT}}(\hbar\omega)$, and $J_{\text{VBT-CBB}}(\hbar\omega)$, respectively, correspond to the integrations of the JDOS integrand, $N_v(E)N_c(E+\hbar\omega)$, between energies $E_{c_\text{D}}-\hbar\omega$ and E_{v_T}, $-\infty$ and $E_{c_\text{D}}-\hbar\omega$, E_{v_T} and $E_{c_\text{T}}-\hbar\omega$, and $E_{c_\text{T}}-\hbar\omega$ and ∞. The JDOS contributions to the overall JDOS function, attributable to these different types of optical transitions, are enumerated next. It is found that

$$J_{\text{VBB-CBT}}(\hbar\omega) = \int_{E_{c_\text{D}}-\hbar\omega}^{E_{v_\text{T}}} N_v(E)\,N_c(E+\hbar\omega)\;dE,$$

$$J_{\text{VBB-CBD}}(\hbar\omega) = \int_{-\infty}^{E_{c_\text{D}}-\hbar\omega} N_v(E)\,N_c(E+\hbar\omega)\;dE,$$

$$J_{\text{VBT-CBT}}(\hbar\omega) = \int_{E_{v_\text{T}}}^{E_{c_\text{T}}-\hbar\omega} N_v(E)\,N_c(E+\hbar\omega)\;dE,$$

$$J_{\text{VBT-CBB}}(\hbar\omega) = \int_{E_{c_\text{T}}-\hbar\omega}^{\infty} N_v(E)\,N_c(E+\hbar\omega)\;dE,$$

$$J_{\text{VBB-CBB}}(\hbar\omega) = 0,$$

and

$$J_{\text{VBT-CBD}}(\hbar\omega) = 0.$$

The third condition, $E_{v_\text{T}} < E_{c_\text{D}}-\hbar\omega$, implies that $\hbar\omega < E_{c_\text{D}}-E_{v_\text{T}}$. The factors in the JDOS integrand are plotted as a function of E for this case in Figure 3.4. For the case of $\hbar\omega < E_{c_\text{D}}-E_{v_\text{T}}$, from Figure 3.4, it is clear that the contributions to the overall JDOS function attributable solely to the VBB-CBD, VBT-CBB, VBT-CBT, and VBT-CBD optical transitions, i.e., $J_{\text{VBB-CBD}}(\hbar\omega)$, $J_{\text{VBT-CBB}}(\hbar\omega)$, $J_{\text{VBT-CBT}}(\hbar\omega)$, and $J_{\text{VBT-CBD}}(\hbar\omega)$, respectively, correspond to the integration of the JDOS integrand, $N_v(E)N_c(E+\hbar\omega)$,

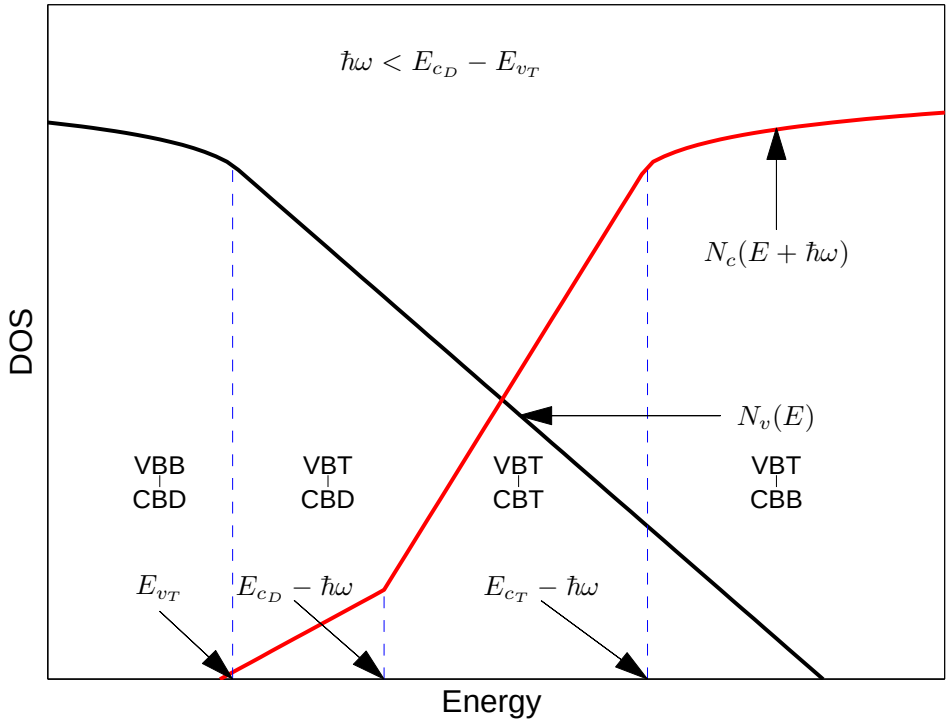

Figure 3.4: The factors in the JDOS integrand, $N_v(E)$ and $N_c(E+\hbar\omega)$, as a function of energy, E, for $\hbar\omega < E_{c_D} - E_{v_T}$. The DOS modeling parameters are as set in Table 3.1.

between energies $-\infty$ and $E_{v_{\mathrm{T}}}$, $E_{c_{\mathrm{T}}}-\hbar\omega$ and ∞, $E_{c_{\mathrm{D}}}-\hbar\omega$ and $E_{c_{\mathrm{T}}}-\hbar\omega$, and $E_{v_{\mathrm{T}}}$ and $E_{c_{\mathrm{D}}}-\hbar\omega$. The JDOS contributions to the overall JDOS function, attributable to these different types of optical transitions, are enumerated next. That is

$$J_{\text{VBB-CBD}}(\hbar\omega)=\int_{-\infty}^{E_{v_{\mathrm{T}}}} N_v(E)\,N_c(E+\hbar\omega)\;dE,$$

$$J_{\text{VBT-CBB}}(\hbar\omega)=\int_{E_{c_{\mathrm{T}}}-\hbar\omega}^{\infty} N_v(E)\,N_c(E+\hbar\omega)\;dE,$$

$$J_{\text{VBT-CBT}}(\hbar\omega)=\int_{E_{c_{\mathrm{D}}}-\hbar\omega}^{E_{c_{\mathrm{T}}}-\hbar\omega} N_v(E)\,N_c(E+\hbar\omega)\;dE,$$

$$J_{\text{VBT-CBD}}(\hbar\omega)=\int_{E_{v_{\mathrm{T}}}}^{E_{c_{\mathrm{D}}}-\hbar\omega} N_v(E)\,N_c(E+\hbar\omega)\;dE,$$

$$J_{\text{VBB-CBB}}(\hbar\omega)=0,$$

and

$$J_{\text{VBB-CBT}}(\hbar\omega)=0.$$

3.2.1 case 1 subcase 1

For the first condition, there are four possible types of optical transitions. In this analysis, the contributions to the overall JDOS function, attributable to those different types of optical transitions, will be derived in closed form.

3.2.1.1 $J_{\text{VBB-CBB}}(\hbar\omega)$

From Figure 3.2, $J_{\text{VBB-CBB}}(\hbar\omega)$, i.e., the contribution to the overall JDOS function attributable to the VBB-CBB optical transitions, may be evaluated

by integrating the JDOS integrand between energies $E_{c_\mathrm{T}}-\hbar\omega$ and E_{v_T}. That is,

$$\begin{aligned} J_{\text{VBB-CBB}}\left(\hbar\omega\right) &= \int_{E_{c_\mathrm{T}}-\hbar\omega}^{E_{v_\mathrm{T}}} N_v\left(E\right) N_c\left(E+\hbar\omega\right)\ dE, \\ &= N_{v_\mathrm{o}} N_{c_\mathrm{o}} \int_{E_{c_\mathrm{T}}-\hbar\omega}^{E_{v_\mathrm{T}}} \sqrt{E_V - E}\sqrt{E+\hbar\omega-E_c}\ dE. \end{aligned}$$

Letting $u = E_v - E$, it is seen that

$$\begin{aligned} J_{\text{VBB-CBB}}\left(\hbar\omega\right) &= N_{v_\mathrm{o}} N_{c_\mathrm{o}} \int_{E_v-E_{c_\mathrm{T}}+\hbar\omega}^{E_v-E_{v_\mathrm{T}}} \sqrt{u}\sqrt{\hbar\omega-(E_c-E_v)-u}\ d(-u), \\ &= N_{v_\mathrm{o}} N_{c_\mathrm{o}} \int_{E_v-E_{v_\mathrm{T}}}^{E_c-E_g-E_{c_\mathrm{T}}+\hbar\omega} \sqrt{u}\sqrt{\hbar\omega-E_g-u}\ du. \end{aligned} \tag{3.5}$$

Again letting $u = (\hbar\omega - E_g)z$, it is found that

$$\begin{aligned} J_{\text{VBB-CBB}}\left(\hbar\omega\right) &= N_{v_\mathrm{o}} N_{c_\mathrm{o}} \int_{\frac{E_v-E_{v_\mathrm{T}}}{\hbar\omega-E_g}}^{\frac{E_c-E_g-E_{c_\mathrm{T}}+\hbar\omega}{\hbar\omega-E_g}} \sqrt{(\hbar\omega-E_g)z} \\ &\qquad \sqrt{(\hbar\omega-E_g)-(\hbar\omega-E_g)z}(\hbar\omega-E_g)z\ dz \\ &= N_{v_\mathrm{o}} N_{c_\mathrm{o}} (\hbar\omega-E_g)^2 \int_{\frac{E_v-E_{v_\mathrm{T}}}{\hbar\omega-E_g}}^{\frac{\hbar\omega-E_g-(E_{c_\mathrm{T}}-E_c)}{\hbar\omega-E_g}} \sqrt{z}\sqrt{1-z}\ dz, \\ &= N_{v_\mathrm{o}} N_{c_\mathrm{o}} (\hbar\omega-E_g)^2\ \mathcal{Y}\left(\frac{E_v-E_{v_\mathrm{T}}}{\hbar\omega-E_g}, 1-\frac{E_{c_\mathrm{T}}-E_c}{\hbar\omega-E_g}\right), \end{aligned}$$

where the dimensionless function

$$\mathcal{Y}(z_1,z_2) \equiv \begin{cases} \int_{z_1}^{z_2} \sqrt{x}\sqrt{1-x}\ dx, & 0 \le z_1 \le z_2 \le 1 \\ 0, & \text{otherwise} \end{cases}. \tag{3.6}$$

This is the same function that is defined in Eq. (11) of O'Leary [20]. The solution for this function is given as,

$$\mathcal{Y}(z_1, z_2) = \begin{cases} \mathcal{Z}(z_2) - \mathcal{Z}(z_1), & 0 \leq z_1 \leq z_2 \leq 1 \\ 0, & \text{otherwise} \end{cases},$$

where

$$\mathcal{Z}(z) = \int_0^z \sqrt{x}\sqrt{1-x}\; dx. \tag{3.7}$$

Through substituting $x = sin^2(\theta)$, it can be shown that

$$\mathcal{Z}(z) = \frac{1}{4}\sin^{-1}(\sqrt{z}) - \frac{1}{4}\sqrt{z}\sqrt{1-z}[1-2z]. \tag{3.8}$$

3.2.1.2 $J_{\text{VBB-CBT}}(\hbar\omega)$

From Figure 3.2, $J_{\text{VBB-CBT}}(\hbar\omega)$, i.e., the contribution to the overall JDOS function attributable to the VBB-CBT optical transitions, may be evaluated by integrating the JDOS integrand between energies $E_{c_\text{D}} - \hbar\omega$ and $E_{c_\text{T}} - \hbar\omega$. That is,

$$\begin{aligned} J_{\text{VBB-CBT}}(\hbar\omega) &= \int_{E_{c_\text{D}}-\hbar\omega}^{E_{c_\text{T}}-\hbar\omega} N_v(E)\, N_c(E+\hbar\omega)\; dE, \\ &= N_{v_\text{o}} N_{c_\text{o}}\; \sqrt{E_{c_\text{T}} - E_c}\; \exp\left(\frac{E_c - E_{c_\text{T}}}{\gamma_c}\right) \\ &\quad \underbrace{\int_{E_{c_\text{D}}-\hbar\omega}^{E_{c_\text{T}}-\hbar\omega} \sqrt{E_v - E}\exp\left(\frac{E+\hbar\omega-E_c}{\gamma_c}\right)\; dE}_{\text{integral}}. \end{aligned} \tag{3.9}$$

For this integral, if one assumes that $u = E_v - E$,

$$= \int_{E_v - E_{c_\mathrm{D}} + \hbar\omega}^{E_v - E_{c_\mathrm{T}} + \hbar\omega} \sqrt{u}\ \exp\left(\frac{E_v - u + \hbar\omega - E_c}{\gamma_c}\right)\ d(-u),$$

$$= \int_{E_v - E_{c_\mathrm{T}} + \hbar\omega}^{E_v - E_{c_\mathrm{D}} + \hbar\omega} \sqrt{u}\ \exp\left(\frac{E_v + \hbar\omega - E_c}{\gamma_c}\right)\ \exp\left(-\frac{u}{\gamma_c}\right)\ du.$$

Letting $\frac{u}{\gamma_c} = z$, this integral transforms into

$$= \gamma_c^{3/2}\ \exp\left(\frac{E_v + \hbar\omega - E_c}{\gamma_c}\right) \int_{\frac{E_v - E_{c_\mathrm{T}} + \hbar\omega}{\gamma_c}}^{\frac{E_v - E_{c_\mathrm{D}} + \hbar\omega}{\gamma_c}} \sqrt{z} \exp(-z)\ dz,$$

$$= \gamma_c^{3/2}\ \exp\left(\frac{E_v + \hbar\omega - E_c}{\gamma_c}\right) \left[\mathrm{Y}\left(\frac{E_v - E_{c_\mathrm{T}} + \hbar\omega}{\gamma_c}\right) - \mathrm{Y}\left(\frac{E_v - E_{c_\mathrm{D}} + \hbar\omega}{\gamma_c}\right)\right],$$

where the dimensionless function,

$$\mathrm{Y}(z) = \int_z^\infty \sqrt{x} \exp(-x)\ dx, \tag{3.10}$$

Using integration by parts, this integration reduces to

$$\mathrm{Y}(z) = \sqrt{z} \exp(-z) + \int_z^\infty \frac{1}{2\sqrt{x}} \exp(-x)\ dx. \tag{3.11}$$

By substituting $x = t^2$, one can obtain

$$\mathrm{Y}(z) = \sqrt{z} \exp(-z) + \frac{\sqrt{\pi}}{2} \mathrm{erfc}(\sqrt{z}), \tag{3.12}$$

where the complementary error function is defined as

$$\mathrm{erfc}(z) \equiv \frac{2}{\sqrt{\pi}} \int_z^\infty \exp(-x^2)\ dx. \tag{3.13}$$

Thus,

$$J_{\text{VBB-CBT}}(\hbar\omega) = N_{v_\text{o}} N_{c_\text{o}} \sqrt{E_{c_\text{T}} - E_c} \exp\left(\frac{E_c - E_{c_\text{T}}}{\gamma_c}\right) \exp\left(\frac{E_v + \hbar\omega - E_c}{\gamma_c}\right) \gamma_c^{3/2} \left[\text{Y}\left(\frac{E_v - E_{c_\text{T}} + \hbar\omega}{\gamma_c}\right) - \text{Y}\left(\frac{E_v - E_{c_\text{D}} + \hbar\omega}{\gamma_c}\right)\right]. \tag{3.14}$$

3.2.1.3 $J_{\text{VBB-CBD}}(\hbar\omega)$

From Figure 3.2, $J_{\text{VBB-CBD}}(\hbar\omega)$, i.e., the contribution to the overall JDOS function attributable to the VBB-CBD optical transitions, may be evaluated by integrating the JDOS integrand between energies $-\infty$ and $E_{c_\text{D}} - \hbar\omega$. That is,

$$\begin{aligned} J_{\text{VBB-CBD}}(\hbar\omega) &= \int_{-\infty}^{E_{c_\text{D}} - \hbar\omega} N_v(E)\, N_c(E + \hbar\omega)\; dE, \\ &= N_{v_\text{o}} N_{c_\text{o}} \sqrt{E_{c_\text{T}} - E_c} \exp\left(\frac{E_c - E_{c_\text{T}}}{\gamma_c}\right) \exp\left(\frac{E_{c_\text{D}} - E_c}{\gamma_c}\right) \underbrace{\int_{-\infty}^{E_{c_\text{D}} - \hbar\omega} \sqrt{E_v - E} \exp\left(\frac{E + \hbar\omega - E_{c_\text{D}}}{\gamma_{c_\text{D}}}\right) dE}_{\text{integral}}. \end{aligned} \tag{3.15}$$

This integral has a similar form to that found in Eq (3.9). Following the same procedure, this integral yields

$$= \gamma_{c_\text{D}}^{3/2} \exp\left(\frac{E_v + \hbar\omega - E_{c_\text{D}}}{\gamma_{c_\text{D}}}\right) \text{Y}\left(\frac{E_v + \hbar\omega - E_{c_\text{D}}}{\gamma_{c_\text{D}}}\right), \tag{3.16}$$

where $\mathrm{Y}(z)$ is the dimensionless function defined in Eq. (3.12). Thus,

$$J_{\text{VBB-CBD}}\left(\hbar\omega\right) = N_{v_{\text{o}}} N_{c_{\text{o}}} \sqrt{E_{c_{\text{T}}} - E_c} \exp\left(\frac{E_c - E_{c_{\text{T}}}}{\gamma_c}\right) \exp\left(\frac{E_{c_{\text{D}}} - E_c}{\gamma_c}\right) \gamma_{c_{\text{D}}}^{3/2} \exp\left(\frac{E_v + \hbar\omega - E_{c_{\text{D}}}}{\gamma_{c_{\text{D}}}}\right) \mathrm{Y}\left(\frac{E_v + \hbar\omega - E_{c_{\text{D}}}}{\gamma_{c_{\text{D}}}}\right). \tag{3.17}$$

3.2.1.4 $J_{\text{VBT-CBB}}\left(\hbar\omega\right)$

From Figure 3.2, $J_{\text{VBT-CBB}}\left(\hbar\omega\right)$, i.e., the contribution to the overall JDOS function attributable to the VBT-CBB optical transitions, may be evaluated by integrating the JDOS integrand between energies $E_{v_{\text{T}}}$ and ∞. That is,

$$\begin{aligned} J_{\text{VBT-CBB}}\left(\hbar\omega\right) &= \int_{E_{v_{\text{T}}}}^{\infty} N_v\left(E\right) N_c\left(E + \hbar\omega\right) \, dE, \\ &= N_{v_{\text{o}}} N_{c_{\text{o}}} \sqrt{E_v - E_{v_{\text{T}}}} \exp\left(\frac{E_{v_{\text{T}}} - E_v}{\gamma_v}\right) \underbrace{\int_{E_{v_{\text{T}}}}^{\infty} \sqrt{E + \hbar\omega - E_c} \exp\left(\frac{E_v - E}{\gamma_v}\right) \, dE}_{\text{integral}}. \end{aligned} \tag{3.18}$$

For this integral, if one assumes that $u = E + \hbar\omega - E_c$, one obtains

$$\exp\left(\frac{E_v - E_c + \hbar\omega}{\gamma_v}\right) \int_{E_{v_{\text{T}}} + \hbar\omega - E_c}^{\infty} \sqrt{u} \exp\left(-\frac{u}{\gamma_v}\right) \, du.$$

Letting $\frac{u}{\gamma_v} = z$, this yields

$$= \gamma_v^{3/2} \exp\left(\frac{E_v - E_c + \hbar\omega}{\gamma_v}\right) \int_{\frac{E_{v_T} + \hbar\omega - E_c}{\gamma_v}}^{\infty} \sqrt{z} \exp(-z)\, dz,$$

$$= \gamma_v^{3/2} \exp\left(\frac{E_v - E_c + \hbar\omega}{\gamma_v}\right) \mathrm{Y}\left(\frac{E_{v_T} + \hbar\omega - E_c}{\gamma_v}\right), \tag{3.19}$$

where $\mathrm{Y}(z)$ is the dimensionless function, defined in Eq. (3.12). Thus,

$$J_{\text{VBT-CBB}}(\hbar\omega) = N_{v_o} N_{c_o} \sqrt{E_v - E_{v_T}} \exp\left(\frac{E_{v_T} - E_v}{\gamma_v}\right) \exp\left(\frac{E_v - E_c + \hbar\omega}{\gamma_v}\right) \gamma_v^{3/2} \mathrm{Y}\left(\frac{E_{v_T} + \hbar\omega - E_c}{\gamma_v}\right). \tag{3.20}$$

3.2.2 Case 1 subcase 2

For the second condition, there are four possible types of optical transitions that have definite values. For this analysis, the contributions to the overall JDOS function, attributable to these different types of optical transitions, will be derived in closed form.

3.2.2.1 $J_{\text{VBB-CBT}}(\hbar\omega)$

From Figure 3.3, $J_{\text{VBB-CBT}}(\hbar\omega)$, i.e., the contribution to the overall JDOS function attributable to the VBB-CBT optical transitions, may be evaluated by integrating the JDOS integrand between energies $E_{c_D} - \hbar\omega$ and E_{v_T}. That is,

$$J_{\text{VBB-CBT}}(\hbar\omega) = \int_{E_{c_{\text{D}}}-\hbar\omega}^{E_{v_{\text{T}}}} N_v(E)\, N_c(E+\hbar\omega)\; dE,$$

$$= N_{v_{\text{o}}} N_{c_{\text{o}}}\; \sqrt{E_{c_{\text{T}}} - E_c}\; \exp\left(\frac{E_c - E_{c_{\text{T}}}}{\gamma_c}\right)$$

$$\underbrace{\int_{E_{c_{\text{D}}}-\hbar\omega}^{E_{v_{\text{T}}}} \sqrt{E_v - E}\; \exp\left(\frac{E+\hbar\omega - E_c}{\gamma_c}\right)\; dE}_{\text{integral}}\,. \tag{3.21}$$

This integral has a similar form to that of Eq (3.9). Following the same procedures, this integral yields,

$$= \gamma_c^{3/2}\; \exp\left(\frac{E_v + \hbar\omega - E_c}{\gamma_c}\right)\; \left[\text{Y}\left(\frac{E_v - E_{v_{\text{T}}}}{\gamma_c}\right) - \text{Y}\left(\frac{E_v + \hbar\omega - E_{c_{\text{D}}}}{\gamma_c}\right)\right], \tag{3.22}$$

where $\text{Y}(z)$ is the dimensionless function defined in Eq. (3.12). Thus,

$$J_{\text{VBB-CBT}}(\hbar\omega) = N_{v_{\text{o}}} N_{c_{\text{o}}}\; \sqrt{E_{c_{\text{T}}} - E_c}\; \exp\left(\frac{E_c - E_{c_{\text{T}}}}{\gamma_c}\right)\; \exp\left(\frac{E_v + \hbar\omega - E_c}{\gamma_c}\right) \tag{3.23}$$

$$\gamma_c^{3/2}\; \left[\text{Y}\left(\frac{E_v - E_{v_{\text{T}}}}{\gamma_c}\right) - \text{Y}\left(\frac{E_v + \hbar\omega - E_{c_{\text{D}}}}{\gamma_c}\right)\right]. \tag{3.24}$$

3.2.2.2 $J_{\text{VBB-CBD}}(\hbar\omega)$

From Figure 3.3, $J_{\text{VBB-CBD}}(\hbar\omega)$, i.e., the contribution to the overall JDOS function attributable to the VBB-CBD optical transitions, may be evaluated by integrating the JDOS integrand between energies $-\infty$ and $E_{c_{\text{D}}} - \hbar\omega$. That

is,

$$J_{\text{VBB-CBD}}(\hbar\omega) = \int_{-\infty}^{E_{c_\text{D}}-\hbar\omega} N_v(E)\, N_c(E+\hbar\omega)\; dE,$$

$$= N_{v_\text{o}} N_{c_\text{o}}\; \sqrt{E_{c_\text{T}} - E_c}\; \exp\left(\frac{E_c - E_{c_\text{T}}}{\gamma_c}\right)\; \exp\left(\frac{E_{c_\text{D}} - E_c}{\gamma_c}\right)$$

$$\underbrace{\int_{-\infty}^{E_{c_\text{D}}-\hbar\omega} \sqrt{E_v - E}\; \exp\left(\frac{E+\hbar\omega - E_{c_\text{D}}}{\gamma_{c_\text{D}}}\right)\; dE}_{\text{integral}}\,. \qquad (3.25)$$

This integral has exactly the same form to that of Eq (3.15). Thus, the result reduces to

$$J_{\text{VBB-CBD}}(\hbar\omega) = N_{v_\text{o}} N_{c_\text{o}}\; \sqrt{E_{c_\text{T}} - E_c}\; \exp\left(\frac{E_c - E_{c_\text{T}}}{\gamma_c}\right)\; \exp\left(\frac{E_{c_\text{D}} - E_c}{\gamma_c}\right) \qquad (3.26)$$

$$\gamma_{c_\text{D}}^{3/2}\; \exp\left(\frac{E_v + \hbar\omega - E_{c_\text{D}}}{\gamma_{c_\text{D}}}\right)\; \text{Y}\left(\frac{E_v + \hbar\omega - E_{c_\text{D}}}{\gamma_{c_\text{D}}}\right), \qquad (3.27)$$

where $\text{Y}(z)$ is the dimensionless function defined in Eq. (3.12).

3.2.2.3 $J_{\text{VBT-CBB}}(\hbar\omega)$

From Figure 3.3, $J_{\text{VBT-CBB}}(\hbar\omega)$, i.e., the contribution to the overall JDOS function attributable to the VBT-CBB optical transitions, may be evaluated by integrating the JDOS integrand between energies $E_{c_\text{T}} - \hbar\omega$ and ∞. That

is,

$$J_{\text{VBT-CBB}}(\hbar\omega) = \int_{E_{c_\text{T}}-\hbar\omega}^{\infty} N_v(E)\, N_c(E+\hbar\omega)\; dE,$$

$$= N_{v_\text{o}} N_{c_\text{o}}\; \sqrt{E_v - E_{v_\text{T}}}\; \exp\left(\frac{E_{v_\text{T}} - E_v}{\gamma_v}\right)$$

$$\underbrace{\int_{E_{c_\text{T}}-\hbar\omega}^{\infty} \sqrt{E+\hbar\omega-E_c}\; \exp\left(\frac{E_v - E}{\gamma_v}\right)\; dE}_{\text{integral}}. \qquad (3.28)$$

This integrand has a similar form to that of Eq (3.18). Following the same procedure, this integral yields

$$= \gamma_v^{3/2}\; \exp\left(\frac{E_v - E_c + \hbar\omega}{\gamma_v}\right)\; \text{Y}\left(\frac{E_{c_\text{T}} - E_c}{\gamma_v}\right), \qquad (3.29)$$

where $\text{Y}(z)$ is the dimensionless function, defined in Eq. (3.12). Thus,

$$J_{\text{VBT-CBB}}(\hbar\omega) = N_{v_\text{o}} N_{c_\text{o}}\; \sqrt{E_v - E_{v_\text{T}}}\; \exp\left(\frac{E_{v_\text{T}} - E_v}{\gamma_v}\right)\; \exp\left(\frac{E_v - E_c + \hbar\omega}{\gamma_v}\right)$$
$$\gamma_v^{3/2}\; \text{Y}\left(\frac{E_{c_\text{T}} - E_c}{\gamma_v}\right). \qquad (3.30)$$

3.2.2.4 $J_{\text{VBT-CBT}}(\hbar\omega)$

From Figure 3.3, $J_{\text{VBT-CBT}}(\hbar\omega)$, i.e., the contribution to the overall JDOS function attributable to the VBT-CBT optical transitions, may be evaluated by integrating the JDOS integrand between energies E_{v_T} and $E_{c_\text{T}} - \hbar\omega$. That is,

$$J_{\text{VBT-CBT}}(\hbar\omega) = \int_{E_{v_\text{T}}}^{E_{c_\text{T}}-\hbar\omega} N_v(E)\, N_c(E+\hbar\omega)\; dE,$$

$$
\begin{aligned}
&= N_{v_\mathrm{o}} N_{c_\mathrm{o}} \sqrt{E_v - E_{v_\mathrm{T}}} \sqrt{E_{c_\mathrm{T}} - E_c} \\
&\quad \exp\left(\frac{E_{v_\mathrm{T}} - E_v}{\gamma_v}\right) \exp\left(\frac{E_c - E_{c_\mathrm{T}}}{\gamma_c}\right) \\
&\quad \int_{E_{v_\mathrm{T}}}^{E_{c_\mathrm{T}} - \hbar\omega} \exp\left(\frac{E_v - E}{\gamma_v}\right) \exp\left(\frac{E + \hbar\omega - E_c}{\gamma_c}\right) \; dE, \\
&= N_{v_\mathrm{o}} N_{c_\mathrm{o}} \sqrt{E_v - E_{v_\mathrm{T}}} \sqrt{E_{c_\mathrm{T}} - E_c} \exp\left(\frac{E_c - E_{c_\mathrm{T}}}{\gamma_c}\right) \\
&\quad \exp\left(\frac{E_{v_\mathrm{T}} - E_v}{\gamma_V}\right) \exp\left(\frac{E_v}{\gamma_v} + \frac{\hbar\omega - E_c}{\gamma_c}\right) \\
&\quad \underbrace{\int_{E_{v_\mathrm{T}}}^{E_{c_\mathrm{T}} - \hbar\omega} \exp\left(\frac{E}{\gamma_c} - \frac{E}{\gamma_v}\right) \; dE}_{\text{integral}} .
\end{aligned}
\tag{3.31}
$$

For this integral, two types of conditions are considered.

For the specific case for which, $\gamma_c = \gamma_v$, this integral reduces to

$$
\begin{aligned}
&\int_{E_{v_\mathrm{T}}}^{E_{c_\mathrm{T}} - \hbar\omega} dE \\
&= E_{c_\mathrm{T}} - \hbar\omega - E_{v_\mathrm{T}}.
\end{aligned}
$$

In contrast, for $\gamma_c \neq \gamma_v$, the integral reduces to

$$
\int_{E_{v_\mathrm{T}}}^{E_{c_\mathrm{T}} - \hbar\omega} \exp\left(\frac{E}{\gamma_c} - \frac{E}{\gamma_v}\right) \; dE,
$$

which is found to be

$$= \frac{1}{\left(\frac{1}{\gamma_c} - \frac{1}{\gamma_v}\right)} \left[\exp\left(\left(E_{c_\mathrm{T}} - \hbar\omega\right)\left(\frac{1}{\gamma_c} - \frac{1}{\gamma_v}\right)\right) - \exp\left(E_{v_\mathrm{T}}\left(\frac{1}{\gamma_c} - \frac{1}{\gamma_v}\right)\right)\right]. \tag{3.32}$$

3.2.3 Case 2

For the third condition, there are four possible types of optical transition to consider. In this analysis, the contributions to the overall JDOS function, attributable to these different types optical transitions, will be obtained.

3.2.3.1 $J_{\mathrm{VBB\text{-}CBD}}(\hbar\omega)$

From Figure 3.4, $J_{\mathrm{VBB\text{-}CBD}}(\hbar\omega)$, i.e., the contribution to the overall JDOS function attributable to the VBB-CBD optical transitions, may be evaluated by integrating the JDOS integrand between energies $-\infty$ and E_{v_T}. That is,

$$\begin{aligned} J_{\mathrm{VBB\text{-}CBD}}(\hbar\omega) &= \int_{-\infty}^{E_{v_\mathrm{T}}} N_v(E)\, N_c(E+\hbar\omega)\; dE, \\ &= N_{v_\mathrm{o}} N_{c_\mathrm{o}}\; \sqrt{E_{c_\mathrm{T}} - E_c}\exp\left(\frac{E_c - E_{c_\mathrm{T}}}{\gamma_c}\right)\; \exp\left(\frac{E_{c_\mathrm{D}} - E_c}{\gamma_c}\right) \\ &\quad \underbrace{\int_{-\infty}^{E_{v_\mathrm{T}}} \sqrt{E_v - E}\exp\left(\frac{E + \hbar\omega - E_{c_\mathrm{D}}}{\gamma_{c_\mathrm{D}}}\right)\; dE}_{\text{integral}}. \end{aligned} \tag{3.33}$$

This integrand has a similar form to that of Eq (3.9). Following the same procedure, this integral yields

$$= \gamma_{c_{\mathrm{D}}}^{3/2} \ \exp\left(\frac{E_v + \hbar\omega - E_{c_{\mathrm{D}}}}{\gamma_{c_{\mathrm{D}}}}\right) \ \mathrm{Y}\left(\frac{E_v - E_{v_{\mathrm{T}}}}{\gamma_{c_{\mathrm{D}}}}\right), \tag{3.34}$$

where $\mathrm{Y}(z)$ is the dimensionless function, defined in Eq. (3.12). Thus,

$$J_{\text{VBB-CBD}}\left(\hbar\omega\right) = N_{v_{\mathrm{o}}} N_{c_{\mathrm{o}}} \ \sqrt{E_{c_{\mathrm{T}}} - E_c} \ \exp\left(\frac{E_c - E_{c_{\mathrm{T}}}}{\gamma_c}\right) \ \exp\left(\frac{E_{c_{\mathrm{D}}} - E_c}{\gamma_c}\right)$$
$$\gamma_{c_{\mathrm{D}}}^{3/2} \ \exp\left(\frac{E_v + \hbar\omega - E_{c_{\mathrm{D}}}}{\gamma_{c_{\mathrm{D}}}}\right) \ \mathrm{Y}\left(\frac{E_v - E_{v_{\mathrm{T}}}}{\gamma_{c_{\mathrm{D}}}}\right). \tag{3.35}$$

3.2.3.2 $J_{\text{VBT-CBB}}\left(\hbar\omega\right)$

From Figure 3.4, $J_{\text{VBT-CBB}}\left(\hbar\omega\right)$, i.e., the contribution to the overall JDOS function attributable to the VBT-CBB optical transitions, may be evaluated by integrating the JDOS integrand between energies $E_{c_{\mathrm{T}}} - \hbar\omega$ and ∞. That is,

$$J_{\text{VBT-CBB}}\left(\hbar\omega\right) = \int_{E_{c_{\mathrm{T}}} - \hbar\omega}^{\infty} N_v\left(E\right) N_c\left(E + \hbar\omega\right) \ dE,$$

$$= N_{v_{\mathrm{o}}} N_{c_{\mathrm{o}}} \ \sqrt{E_v - E_{v_{\mathrm{T}}}} \ \exp\left(\frac{E_{v_{\mathrm{T}}} - E_v}{\gamma_v}\right)$$
$$\underbrace{\int_{E_{c_{\mathrm{T}}} - \hbar\omega}^{\infty} \sqrt{E + \hbar\omega - E_c} \ \exp\left(\frac{E_v - E}{\gamma_v}\right) \ dE}_{\text{integral}}. \tag{3.36}$$

This integral has exactly the same form as that associated with Eq (3.28). Thus, this contribution may be expressed as

$$J_{\text{VBT-CBB}}\left(\hbar\omega\right) = N_{v_{\text{o}}} N_{c_{\text{o}}}\ \sqrt{E_v - E_{v_{\text{T}}}}\ \exp\left(\frac{E_{v_{\text{T}}} - E_v}{\gamma_v}\right)\ \exp\left(\frac{E_v - E_c + \hbar\omega}{\gamma_v}\right)$$
$$\gamma_v^{3/2}\ \text{Y}\left(\frac{E_{c_{\text{T}}} - E_c}{\gamma_v}\right), \tag{3.37}$$

where $\text{Y}(z)$ is the dimensionless function, defined in Eq. (3.12).

3.2.3.3 $J_{\text{VBT-CBT}}\left(\hbar\omega\right)$

From Figure 3.4, $J_{\text{VBT-CBT}}\left(\hbar\omega\right)$, i.e., the contribution to the overall JDOS function attributable to the VBT-CBT optical transitions, may be evaluated by integrating the JDOS integrand between energies $E_{c_{\text{D}}} - \hbar\omega$ and $E_{c_{\text{T}}} - \hbar\omega$. That is,

$$J_{\text{VBT-CBT}}\left(\hbar\omega\right) = \int_{E_{c_{\text{D}}} - \hbar\omega}^{E_{c_{\text{T}}} - \hbar\omega} N_v\left(E\right) N_c\left(E + \hbar\omega\right)\ dE,$$
$$= N_{v_{\text{o}}} N_{c_{\text{o}}}\ \sqrt{E_v - E_{v_{\text{T}}}}\ \sqrt{E_{c_{\text{T}}} - E_c}\ \exp\left(\frac{E_c - E_{c_{\text{T}}}}{\gamma_c}\right)$$
$$\exp\left(\frac{E_{v_{\text{T}}} - E_v}{\gamma_V}\right)\ \exp\left(\frac{E_v}{\gamma_v} + \frac{\hbar\omega - E_c}{\gamma_c}\right)$$
$$\underbrace{\int_{E_{c_{\text{D}}} - \hbar\omega}^{E_{c_{\text{T}}} - \hbar\omega} \exp\left(\frac{E}{\gamma_c} - \frac{E}{\gamma_v}\right)\ dE}_{\text{integral}}. \tag{3.38}$$

For this integral, two types of conditions are considered.

For the specific case for which $\gamma_c = \gamma_v$, this integral reduces to

$$\int_{E_{c_\mathrm{D}}-\hbar\omega}^{E_{c_\mathrm{T}}-\hbar\omega} dE = E_{c_\mathrm{T}} - \hbar\omega - E_{c_\mathrm{D}} + \hbar\omega,$$

$$= E_{c_\mathrm{T}} - E_{c_\mathrm{D}}. \tag{3.39}$$

In contrast, for $\gamma_c \neq \gamma_v$, the integral reduces to

$$\int_{E_{c_\mathrm{D}}-\hbar\omega}^{E_{c_\mathrm{T}}-\hbar\omega} \exp\left(\frac{E}{\gamma_c} - \frac{E}{\gamma_v}\right)\ dE,$$

which is found to be

$$= \frac{1}{\left(\frac{1}{\gamma_c} - \frac{1}{\gamma_v}\right)} \left[\exp\left((E_{c_\mathrm{T}} - \hbar\omega)\left(\frac{1}{\gamma_c} - \frac{1}{\gamma_v}\right)\right) - \exp\left((E_{c_\mathrm{D}} - \hbar\omega)\left(\frac{1}{\gamma_c} - \frac{1}{\gamma_v}\right)\right)\right]. \tag{3.40}$$

3.2.3.4 $J_{\text{VBT-CBD}}(\hbar\omega)$

From Figure 3.4, $J_{\text{VBT-CBD}}(\hbar\omega)$, i.e., the contribution to the overall JDOS function attributable to the VBT-CBD optical transitions, may be evaluated by integrating the JDOS integrand between energies E_{v_T} and $E_{c_\mathrm{D}} - \hbar\omega$. That is,

$$J_{\text{VBT-CBD}}(\hbar\omega) = \int_{E_{v_\mathrm{T}}}^{E_{c_\mathrm{D}}-\hbar\omega} N_v(E)\, N_c(E+\hbar\omega)\ dE,$$

$$= N_{v_\mathrm{o}} N_{c_\mathrm{o}}\ \sqrt{E_v - E_{v_\mathrm{T}}}\ \sqrt{E_{c_\mathrm{T}} - E_c}\ \exp\left(\frac{E_c - E_{c_\mathrm{T}}}{\gamma_c}\right)$$

$$\exp\left(\frac{E_{v_{\mathrm{T}}}-E_v}{\gamma_V}\right)\ \exp\left(\frac{E_{c_{\mathrm{D}}}-E_c}{\gamma_c}\right)\ \exp\left(\frac{E_v}{\gamma_v}+\frac{\hbar\omega-E_{c_{\mathrm{D}}}}{\gamma_{c_{\mathrm{D}}}}\right)$$
$$\underbrace{\int_{E_{v_{\mathrm{T}}}}^{E_{c_{\mathrm{D}}}-\hbar\omega}\exp\left(\frac{E}{\gamma_{c_{\mathrm{D}}}}-\frac{E}{\gamma_v}\right)\ dE}_{\text{integral}}. \tag{3.41}$$

For this integral, two types of conditions are considered.

For the specific case for which $\gamma_{c_{\mathrm{D}}}=\gamma_v$, this integral reduces to

$$\int_{E_{v_{\mathrm{T}}}}^{E_{c_{\mathrm{D}}}-\hbar\omega} dE = E_{c_{\mathrm{D}}}-\hbar\omega-E_{v_{\mathrm{T}}}. \tag{3.42}$$

In contrast, for $\gamma_{c_{\mathrm{D}}}\neq\gamma_v$, this integral reduces to

$$\int_{E_{v_{\mathrm{T}}}}^{E_{c_{\mathrm{D}}}-\hbar\omega}\exp\left(\frac{E}{\gamma_{c_{\mathrm{D}}}}-\frac{E}{\gamma_v}\right)\ dE, \tag{3.43}$$

which is found to be

$$=\frac{1}{\left(\frac{1}{\gamma_{c_{\mathrm{D}}}}-\frac{1}{\gamma_v}\right)}\left[\exp\left((E_{c_{\mathrm{D}}}-\hbar\omega)\left(\frac{1}{\gamma_{c_{\mathrm{D}}}}-\frac{1}{\gamma_v}\right)\right)-\exp\left(E_{v_{\mathrm{T}}}\left(\frac{1}{\gamma_{c_{\mathrm{D}}}}-\frac{1}{\gamma_v}\right)\right)\right]. \tag{3.44}$$

3.3 Valence band defect model

For this case, a distribution of valence band defect states is considered instead. As with the approach for the conduction band defect distribution, for this case, a distribution of valence band defect (VBD) states is added to the distributions of VBB, VBT, CBB and CBT states that were considered by Malik and O'Leary [18]. For this added defect distribution, optical transitions, from the valence band defect to the conduction band band (VBD-CBB) states and from the valence band defect to the conduction band tail (VBD-CBT) states, are to be considered along with the VBB-CBB, VBB-CBT, VBT-VBB and VBT-CBT optical transitions. The empirical valence band DOS defect model may thus be expressed as

$$N_v(E) = N_{vo} \begin{cases} \sqrt{E_v - E_{v_\mathrm{T}}}\ \exp\left(\frac{E_{v_\mathrm{T}} - E_v}{\gamma_v}\right) \exp\left(\frac{E_v - E_{v_\mathrm{D}}}{\gamma_v}\right) & \\ \exp\left(\frac{E_{v_\mathrm{D}} - E}{\gamma_{v_\mathrm{D}}}\right), & E > E_{v_\mathrm{D}} \\ \sqrt{E_v - E_{v_\mathrm{T}}}\ \exp\left(\frac{E_{v_\mathrm{T}} - E_v}{\gamma_v}\right)\ \exp\left(\frac{E_v - E}{\gamma_v}\right), & E_{v_\mathrm{D}} \geq E > E_{v_\mathrm{T}} \\ \sqrt{E_v - E}, & E \leq E_{v_\mathrm{T}} \end{cases}, \tag{3.45}$$

and

$$N_c(E) = N_{co} \begin{cases} \sqrt{E - E_c}, & E \geq E_{c_\mathrm{T}} \\ \sqrt{E_{c_\mathrm{T}} - E_c}\ \exp\left(\frac{E_c - E_{c_\mathrm{T}}}{\gamma_c}\right)\ \exp\left(\frac{E - E_c}{\gamma_c}\right), & E < E_{c_\mathrm{T}} \end{cases}, \tag{3.46}$$

where N_{vo} and N_{co} denote the valence band and conduction band DOS prefactors, respectively, E_v and E_c represent the valence band and conduction band band edges, γ_v and $\gamma_{v_{\mathrm{D}}}$ are the breadths of the valence band tail and valence band defect distributions, γ_c is the breadth of conduction band tail, $E_{v_{\mathrm{T}}}$ and $E_{c_{\mathrm{T}}}$ being the critical energies at which the exponential and square-root distributions interface, $E_{v_{\mathrm{D}}}$ being the critical energy at which the valence band exponential and defect distributions interface; it should be noted that this model implicitly requires that $E_v - E_{v_{\mathrm{T}}} \geq 0$ and that $E_{c_{\mathrm{T}}} - E_c \geq 0$. From Eqs. (3.45) and (3.46), it is noted that $N_v(E)$ and $N_c(E)$ are continuous functions of energy. It is assumed that $\gamma_{v_{\mathrm{D}}} \geq \gamma_v$, and that $E_{v_{\mathrm{D}}} > E_{v_{\mathrm{T}}}$ for the purposes of this analysis. The same nominal a-Si DOS modeling parameters, tabulated in Table 1 of Thevaril and O'Leary [19], are also employed for this analysis. These values are tabulated in Table 3.2, the corresponding DOS functions being as depicted in Figure 3.5. From this figure, it is clear that there are six different types of optical transitions that are possible: (1) VBB-CBB optical transitions, (2) VBB-CBT optical transitions, (3) VBT-CBB optical transitions, (4) VBT-CBT optical transitions, (5) VBD-CBB optical transitions, and (6) VBD-CBT optical transitions.

In order to understand how these optical transitions contribute to the overall optical response of a material, it is necessary to find the JDOS

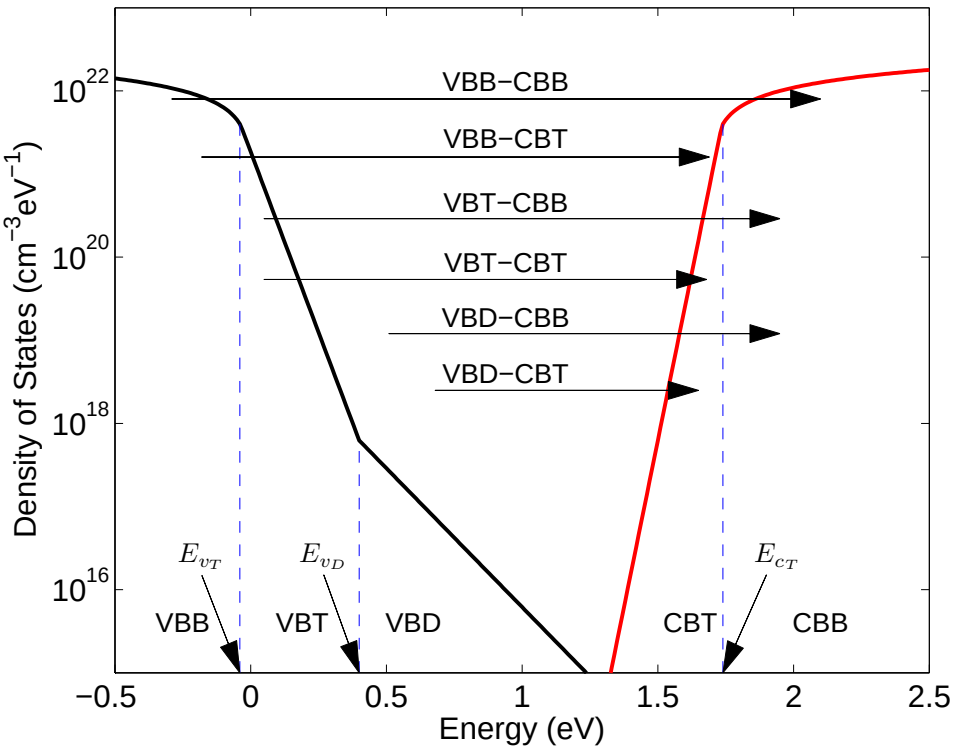

Figure 3.5: The valence band and conduction band DOS functions associated with a-Si. The critical energies in the DOS functions, i.e., E_{v_T}, E_{c_T}, and E_{c_D}, are clearly marked with the dashed lines and the arrows. All the possible optical transitions are shown with the arrows. The DOS modeling parameters are as set in Table 3.2.

Table 3.2: The nominal a-Si DOS modeling parameter selections employed for the purposes of this analysis.

ParameterParameters(units)	Value
N_{vo} ($\mathrm{cm}^{-3}\mathrm{eV}^{-3/2}$)	2×10^{22}
N_{co} ($\mathrm{cm}^{-3}\mathrm{eV}^{-3/2}$)	2×10^{22}
E_v (eV)	0
E_c (eV)	1.7
γ_v (meV)	50
γ_c (meV)	27
$E_v - E_{v_\mathrm{T}}$ (meV)	35
$E_{c_\mathrm{T}} - E_c$ (meV)	35
γ_{v_D} (meV)	130
$E_{v_\mathrm{D}} - E_v$ (meV)	400

contribution corresponding to these six transitions. Three different cases are considered,i.e.,

1. case 1 $E_{v_\mathrm{T}} > E_{c_\mathrm{T}} - \hbar\omega$,

2. case 2 $E_{v_\mathrm{T}} < E_{c_\mathrm{T}} - \hbar\omega < E_{v_\mathrm{D}}$,

and

3. case 3 $E_{v_\mathrm{D}} < E_{c_\mathrm{T}} - \hbar\omega$.

The first condition, $E_{v_\mathrm{T}} > E_{c_\mathrm{T}} - \hbar\omega$, implies that $\hbar\omega > E_{c_\mathrm{T}} - E_{v_\mathrm{T}}$. The factors in the JDOS integrand are plotted as a function of E for this case in Figure 3.6. For the case of $\hbar\omega > E_{c_\mathrm{T}} - E_{v_\mathrm{T}}$, it is clear that VBB-CBB, VBB-CBT, VBT-CBB, and VBD-CBB optical transitions contribute to the overall JDOS function. These optical transitions are denoted $J_{\text{VBB-CBB}}(\hbar\omega)$, $J_{\text{VBB-CBT}}(\hbar\omega)$, $J_{\text{VBT-CBB}}(\hbar\omega)$, and $J_{\text{VBD-CBB}}(\hbar\omega)$, respectively,

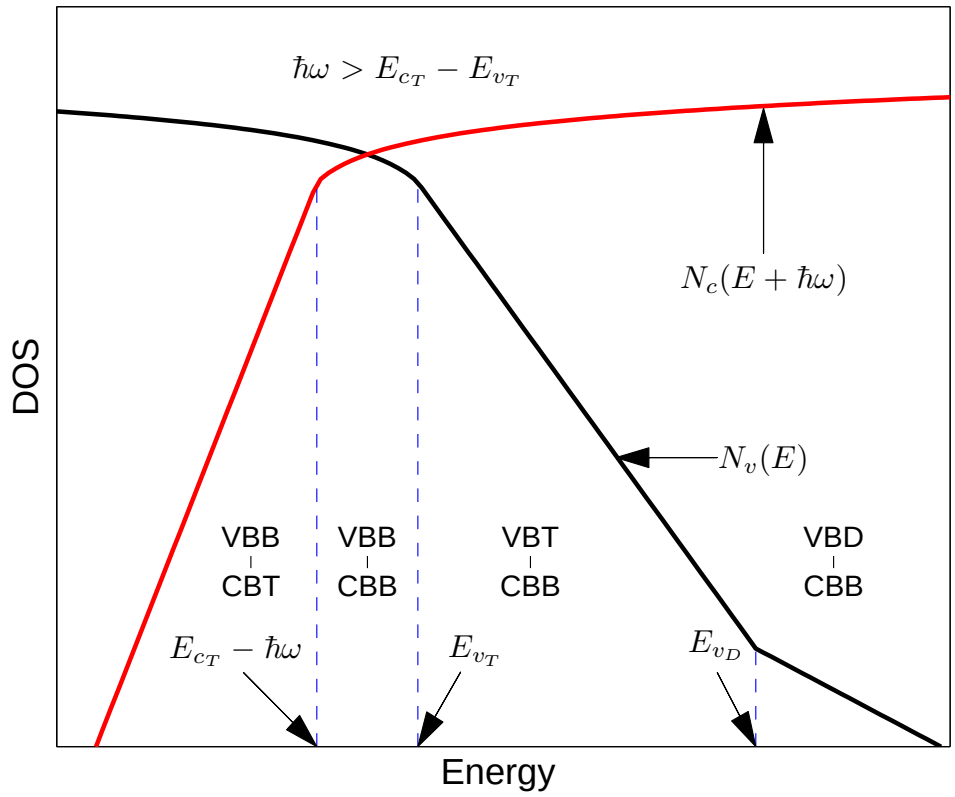

Figure 3.6: The factors in the JDOS integrand, $N_v(E)$ and $N_c(E+\hbar\omega)$, as a function of energy, E, for $\hbar\omega > E_{c_T} - E_{v_T}$. The DOS modeling parameters are as set in Table 3.2.

and these correspond to the integration of the JDOS integrand, $N_v(E)N_c(E+\hbar\omega)$, between energies $E_{c_\mathrm{T}}-\hbar\omega$ and E_{v_T}, $-\infty$ and $E_{c_\mathrm{T}}-\hbar\omega$, E_{v_T} and E_{v_D}, and E_{v_D} and ∞. The JDOS contributions to the overall JDOS function, attributable to these different types of optical transitions, are enumerated below. That is,

$$J_{\text{VBB-CBB}}(\hbar\omega) = \int_{E_{c_\mathrm{T}}-\hbar\omega}^{E_{v_\mathrm{T}}} N_v(E)\, N_c(E+\hbar\omega)\; dE,$$

$$J_{\text{VBB-CBT}}(\hbar\omega) = \int_{-\infty}^{E_{c_\mathrm{T}}-\hbar\omega} N_v(E)\, N_c(E+\hbar\omega)\; dE,$$

$$J_{\text{VBT-CBB}}(\hbar\omega) = \int_{E_{v_\mathrm{T}}}^{E_{v_\mathrm{D}}} N_v(E)\, N_c(E+\hbar\omega)\; dE,$$

$$J_{\text{VBD-CBB}}(\hbar\omega) = \int_{E_{v_\mathrm{D}}}^{\infty} N_v(E)\, N_c(E+\hbar\omega)\; dE,$$

$$J_{\text{VBT-CBT}}(\hbar\omega) = 0,$$

and

$$J_{\text{VBD-CBT}}(\hbar\omega) = 0.$$

The second condition, $E_{v_\mathrm{T}} < E_{c_\mathrm{T}} - \hbar\omega < E_{v_\mathrm{D}}$ implies that $E_{c_\mathrm{T}} - E_{v_\mathrm{D}} < \hbar\omega < E_{c_\mathrm{T}} - E_{v_\mathrm{T}}$. The factors in the JDOS integrand, plotted as a function of E for this case, are depicted in Figure 3.7. For the case of $E_{c_\mathrm{T}} - E_{v_\mathrm{D}} < \hbar\omega < E_{c_\mathrm{T}} - E_{v_\mathrm{T}}$, from Figure 3.7 it is clear that the contributions to the overall JDOS function, attributable solely to the VBB-CBT, VBT-CBB, VBT-CBT, and VBD-CBB optical transitions, i.e., $J_{\text{VBB-CBT}}(\hbar\omega)$, $J_{\text{VBT-CBB}}(\hbar\omega)$, $J_{\text{VBT-CBT}}(\hbar\omega)$, and $J_{\text{VBD-CBB}}(\hbar\omega)$, respectively, correspond to the integrations of the JDOS integrand, $N_v(E)N_c(E+\hbar\omega)$, between

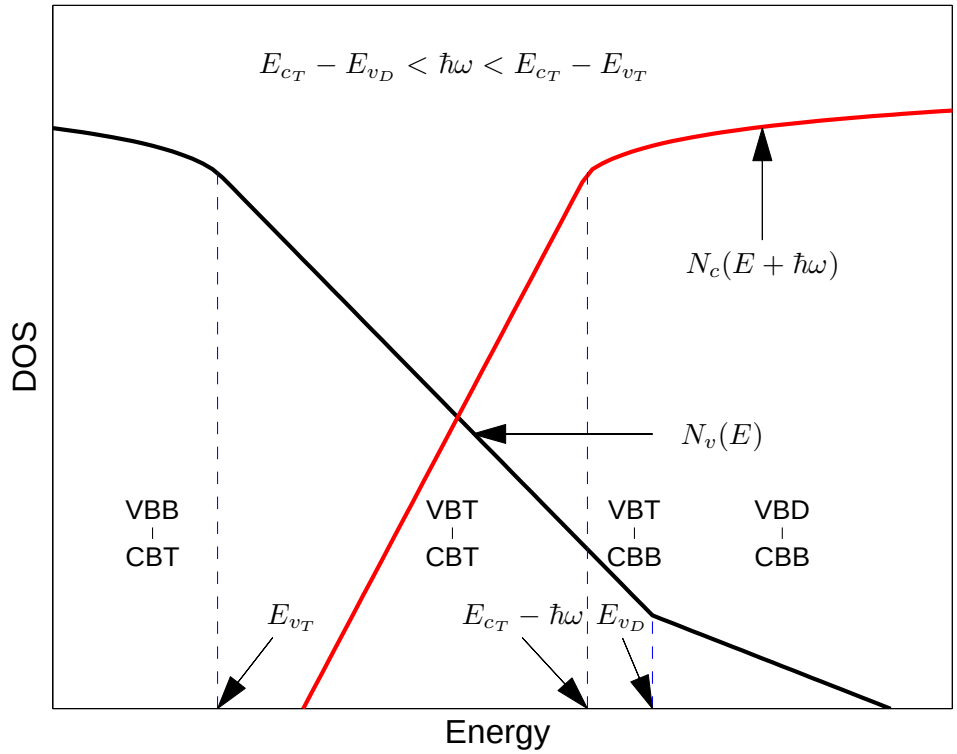

Figure 3.7: The factors in the JDOS integrand, $N_v(E)$ and $N_c(E+\hbar\omega)$, as a function of energy, E, for $E_{c_\mathrm{T}} - E_{v_\mathrm{D}} < \hbar\omega < E_{c_\mathrm{T}} - E_{v_\mathrm{T}}$. The DOS modeling parameters are as set in Table 3.2.

energies $-\infty$ and $E_{v_{\mathrm{T}}}$, $E_{c_{\mathrm{T}}} - \hbar\omega$ and $E_{v_{\mathrm{D}}}$, $E_{v_{\mathrm{T}}}$ and $E_{c_{\mathrm{T}}} - \hbar\omega$, and $E_{v_{\mathrm{D}}}$ and ∞. The JDOS contributions to the overall JDOS function, attributable to these different types of optical transitions, are enumerated below. That is,

$$J_{\text{VBB-CBT}}(\hbar\omega) = \int_{-\infty}^{E_{v_{\mathrm{T}}}} N_v(E)\, N_c(E+\hbar\omega)\; dE,$$

$$J_{\text{VBT-CBT}}(\hbar\omega) = \int_{E_{v_{\mathrm{T}}}}^{E_{c_{\mathrm{T}}}-\hbar\omega} N_v(E)\, N_c(E+\hbar\omega)\; dE,$$

$$J_{\text{VBD-CBB}}(\hbar\omega) = \int_{E_{v_{\mathrm{D}}}}^{\infty} N_v(E)\, N_c(E+\hbar\omega)\; dE,$$

$$J_{\text{VBB-CBB}}(\hbar\omega) = 0,$$

and

$$J_{\text{VBD-CBT}}(\hbar\omega) = 0.$$

The third condition, $E_{v_{\mathrm{D}}} < E_{c_{\mathrm{T}}} - \hbar\omega$, implies that $\hbar\omega < E_{c_{\mathrm{T}}} - E_{v_{\mathrm{D}}}$. The factors in the JDOS integrand, plotted as a function of E for this case, are depicted in Figure 3.8. For the case of $\hbar\omega < E_{c_{\mathrm{T}}} - E_{v_{\mathrm{D}}}$, from Figure 3.8, it is clear that the contributions to the overall JDOS function, attributable solely to the VBB-CBT, VBT-CBT, VBD-CBB, and VBD-CBT optical transitions, i.e., $J_{\text{VBB-CBT}}(\hbar\omega)$, $J_{\text{VBT-CBT}}(\hbar\omega)$, $J_{\text{VBD-CBB}}(\hbar\omega)$, and $J_{\text{VBD-CBT}}(\hbar\omega)$, respectively, correspond to the integrations of the JDOS integrand, $N_v(E)N_c(E+\hbar\omega)$, between energies $-\infty$ and $E_{v_{\mathrm{T}}}$, $E_{v_{\mathrm{T}}}$ and $E_{v_{\mathrm{D}}}$, $E_{c_{\mathrm{T}}} - \hbar\omega$ and ∞, and $E_{v_{\mathrm{D}}}$ and $E_{c_{\mathrm{T}}} - \hbar\omega$. The JDOS contributions to the overall JDOS function, attributable to these different types of optical transitions, are enumerated below. That is,

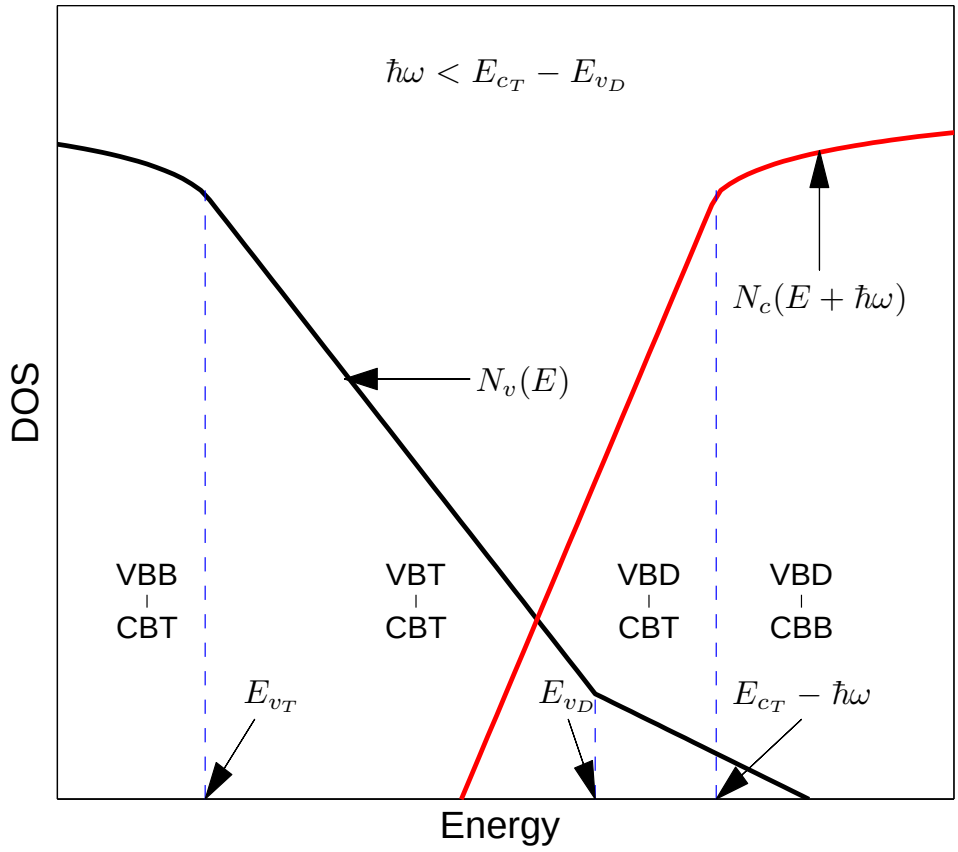

Figure 3.8: The factors in the JDOS integrand, $N_v(E)$ and $N_c(E+\hbar\omega)$, as a function of energy, E, for $\hbar\omega < E_{c_T} - E_{v_D}$. The DOS modeling parameters are as set in Table 3.2.

$$J_{\text{VBB-CBT}}(\hbar\omega) = \int_{-\infty}^{E_{v_{\text{T}}}} N_v(E)\, N_c(E+\hbar\omega)\ dE,$$

$$J_{\text{VBT-CBT}}(\hbar\omega) = \int_{E_{v_{\text{T}}}}^{E_{v_{\text{D}}}} N_v(E)\, N_c(E+\hbar\omega)\ dE,$$

$$J_{\text{VBD-CBB}}(\hbar\omega) = \int_{E_{c_{\text{T}}}-\hbar\omega}^{\infty} N_v(E)\, N_c(E+\hbar\omega)\ dE,$$

$$J_{\text{VBD-CBT}}(\hbar\omega) = \int_{E_{v_{\text{D}}}}^{E_{c_{\text{T}}}-\hbar\omega} N_v(E)\, N_c(E+\hbar\omega)\ dE,$$

$$J_{\text{VBB-CBB}}(\hbar\omega) = 0,$$

and

$$J_{\text{VBT-CBB}}(\hbar\omega) = 0.$$

Analytical results, for the valence band defect model, yield similar expressions to those of the conduction band defect model. One can easily derive these expressions for the three different cases following the same procedures, as discussed previously.

Chapter 4

Application of the conduction band defect and valence band defect models to the analysis of the optical response of a-Si

4.1 Introduction

The presence of defect states will lead to a distinctive broadening exhibited in the sub-gap region of the imaginary part of the dielectric function, $\epsilon_2(E)$, associated with a-Si. For many years, there has been some basic work performed on understanding the optical response of a-Si. With experimen-

tal optical response results for a-Si, models have been proposed to fit the results. In Figure 4.1, a fit is shown with the experimental results of Jackson *et al.* [6], where it is seen that the spectral dependence of the JDOS function, $J(E)$, does not follow the a-Si experimental result for photon energies below 1.4 eV; this evaluation of the JDOS function is performed without the presence of defect state being taken into account. Adding an exponential distribution of defect states onto the intrinsic exponential distribution of tail states can account for this discrepancy.

In this chapter, results produced from the proposed models, i.e., the valence band defect model and the conduction band defect model, are fit to those of experiment. In addition to that, the underlying distribution of defect states that shape the resultant optical response, and the role that the individual types of optical transitions play in determining the behavior of the optical response of these materials, are assessed.

This chapter is organized in the following manner. In Section 4.2, a comparison between the results obtained through the proposed defect model with those obtained with the non-defect model is provided. Then, in Section 4.4, a fit with the result of experiments for the valence band defect model, is shown. In Section 4.3, a fit with the results of experiment, for the conduction band defect model, is discussed. Finally, the uniqueness of the fits to the

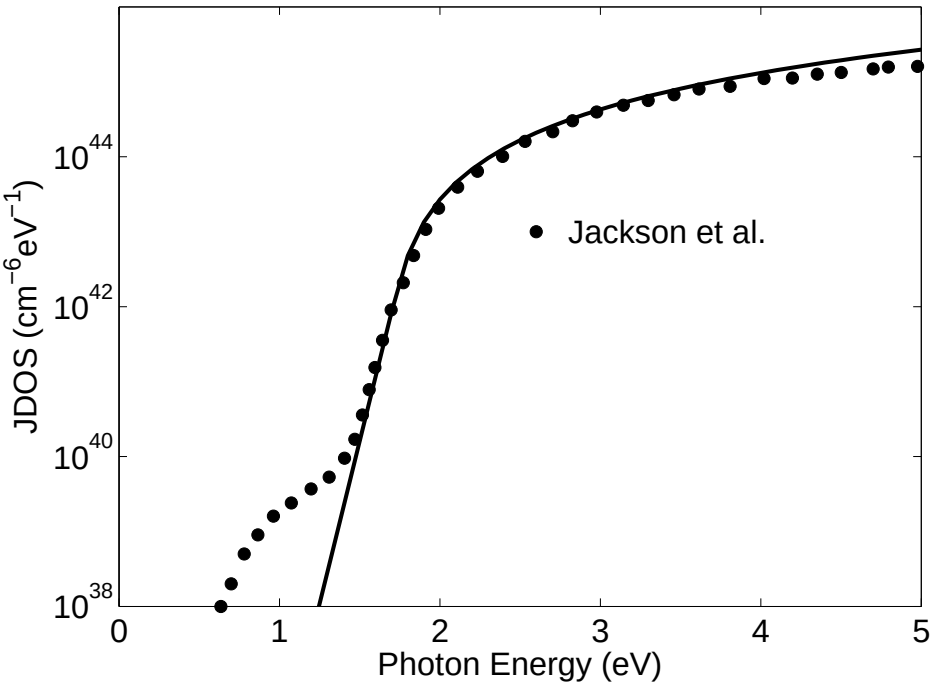

Figure 4.1: The fitting of the spectral dependence of JDOS function. The experimental a-Si JDOS result of Jackson *et al.* [6] is depicted with solid points. The JDOS fit result, obtained by setting $N_{vo} = N_{co} = 2.48 \times 10^{22}\text{cm}^{-3}\text{eV}^{-3/2}$, $E_v = 0.0$ eV, $E_c = 1.68$ eV, and $\gamma_v = 40$ meV, is depicted with the solid line. This figure is after Minar [21].

experimental results considered is commented upon in Section 4.5.

4.2 Comparison between models

To clearly demonstrate how the presence of defects influences the JDOS function, the JDOS functions, with and without defect states taken into account, are plotted in Figure 4.2. The valence band defect JDOS model is compared with defect-free JDOS model, given in Eqs (3.1) and (3.2). It is clear that, in the absence of defect states, an algebraic functional dependence is visible in the band region and an exponential functional dependence is apparent in the sub-gap region, i.e., for $\hbar\omega < E_{c_{\mathrm{T}}} - E_{v_{\mathrm{T}}}$, the breadth of this region being dominated by the tail breadth, γ_v. In the valence band defect model, with defect states included, the corresponding JDOS function broadens considerably at lower photon energies. This significant broadening happens due to optical transitions involving VBD states, i.e., $\hbar\omega < E_{c_{\mathrm{T}}} - E_{v_{\mathrm{D}}}$, and the breadth of this region is dominated by the defect distribution breadth, $\gamma_{v_{\mathrm{D}}}$, for the nominal selection of DOS modeling parameters.

In order to quantitatively investigate the influence of each type of optical transition on the overall JDOS function associated with a-Si, the fractional contributions to the JDOS function related to the conduction band defect model are depicted in Figure 4.3, the fractional contributions to the JDOS

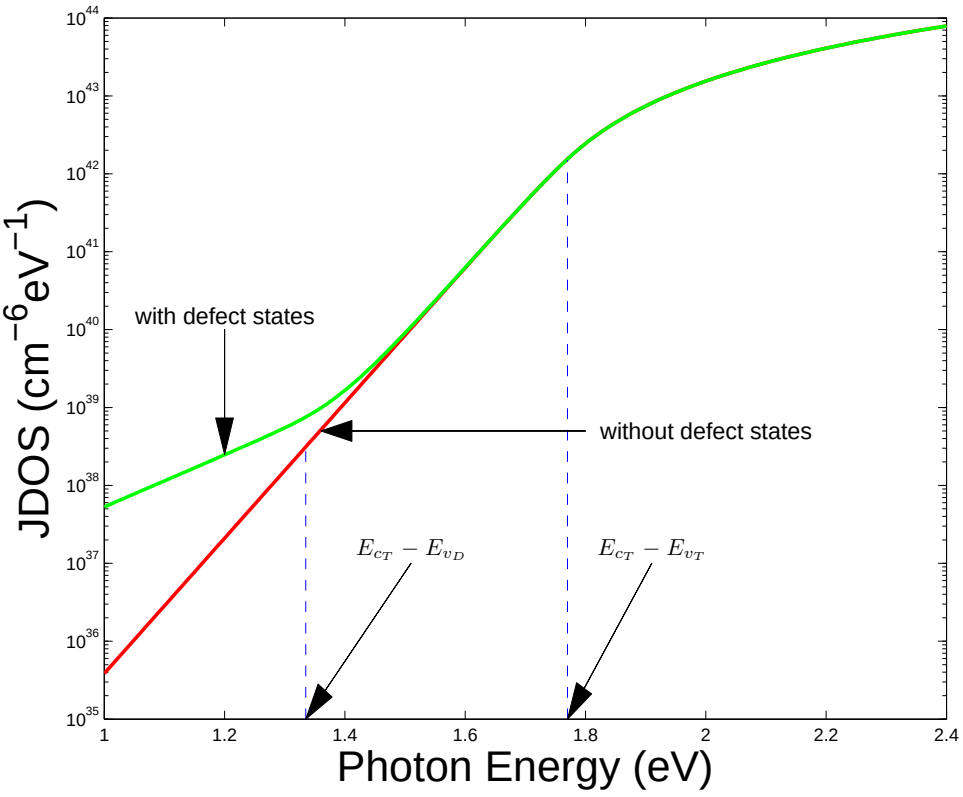

Figure 4.2: A comparison between two JDOS functions, $J(E)$, associated with a-Si, determined through an evaluation of Eq (2.13), are shown in this figure. For the defect-free model, the DOS functions, $N_v(E)$ and $N_c(E)$, are as specified in Eqs. (3.1) and (3.2), respectively. For a model with defect states included, $N_v(E)$ and $N_c(E)$ are as specified in Eqs. (3.45) and (3.46), respectively. $E_{c_T} - E_{v_D}$ and $E_{c_T} - E_{v_T}$, critical energies in the JDOS analysis, are clearly marked with the dashed lines and the arrows. The DOS modeling parameters are as set in Table 3.1.

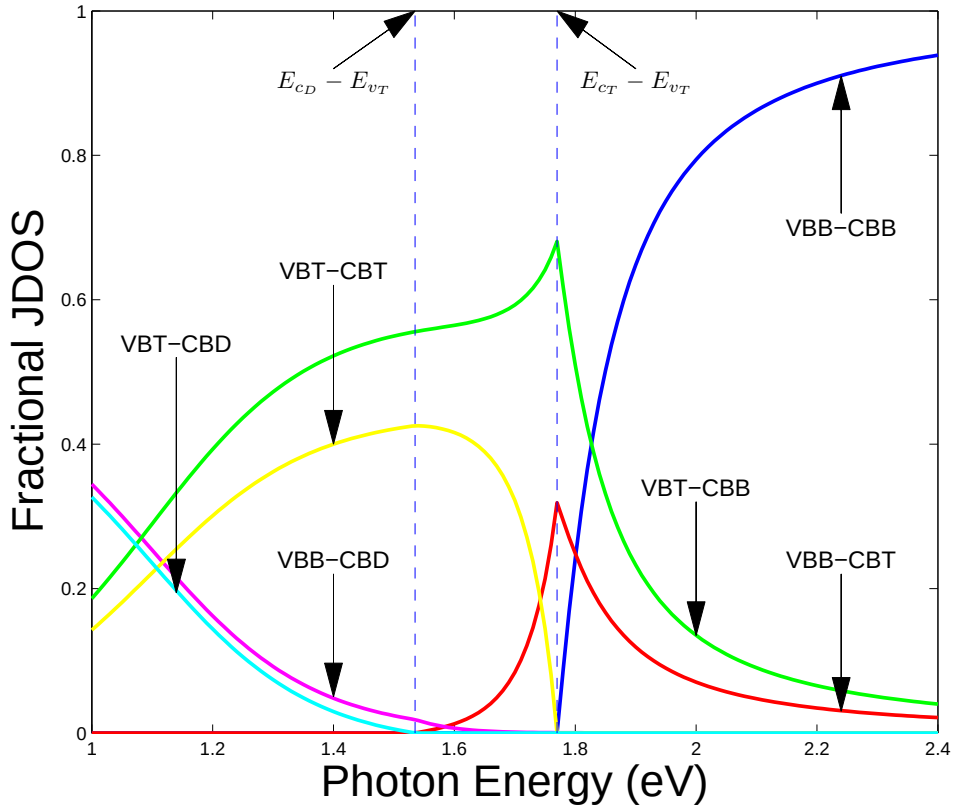

Figure 4.3: The fractional contributions to the overall JDOS function associated with the various types of a-Si optical transitions for the conduction band defect model. $E_{c_\mathrm{D}} - E_{v_\mathrm{T}}$ and $E_{c_\mathrm{T}} - E_{v_\mathrm{T}}$, critical energies in the JDOS analysis, are clearly marked with the dashed lines and the arrows. The DOS modeling parameters are as set in Table 3.1.

function related to the valence band defect model being depicted in Figure 4.4.

In Figure 4.3, for the conduction band defect model, the fractional contributions of the VBB-CBB, VBB-CBT, VBT-CBB, VBT-CBT, VBT-CBD, and VBB-CBD optical transitions to the overall JDOS function, are plotted as a function of photon energy, E. The DOS modeling parameters are set to their nominal a-Si values for the purposes of this analysis, i.e., as set in Table 3.1. The VBB-CBB optical transition contribution to the overall JDOS function is shown with the solid blue line. The VBT-CBB optical transition contribution to the overall JDOS function is shown with the solid green line. The VBB-CBT optical transition contribution to the overall JDOS function is shown with the solid red line. The VBT-CBT optical transition contribution to the overall JDOS function is shown with the solid yellow line. The VBB-CBD optical transition contribution to the overall JDOS function is shown with the solid purple line. The VBT-CBD optical transition contribution to the overall JDOS function is shown with the light blue line. Again, one should note that for the selection of $\hbar\omega$ well above the optical gap, i.e., $\hbar\omega > E_{c_{\mathrm{T}}} - E_{v_{\mathrm{T}}}$, the contribution to the overall JDOS function attributable to VBB-CBB optical transitions increases monotonically with increasing $\hbar\omega$, and it is the dominant type of optical transition in this region, this

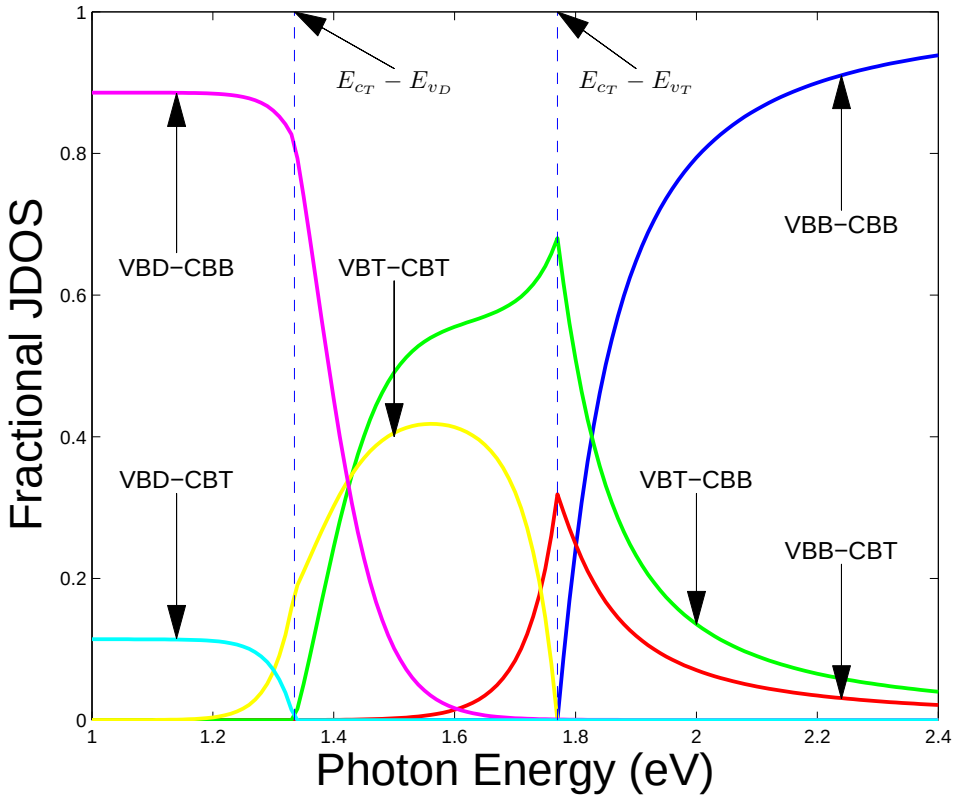

Figure 4.4: The fractional contributions to the overall JDOS function associated with the various types of a-Si optical transitions for the valence band defect model. $E_{c_T} - E_{v_D}$ and $E_{c_T} - E_{v_T}$, critical energies in the JDOS analysis, are clearly marked with the dashed lines and the arrows. The DOS modeling parameters are as set in Table 3.2.

contribution being nil below the optical gap, i.e., for $\hbar\omega < E_{c_{\mathrm{T}}} - E_{v_{\mathrm{T}}}$. In the sub-gap region, i.e., $\hbar\omega < E_{c_{\mathrm{T}}} - E_{v_{\mathrm{D}}}$, VBT-CBB, and VBT-CBT optical transitions are the dominant contributors to the overall JDOS function. On the other hand, VBT-CBD and VBB-CBD optical transitions make small contributions to the overall JDOS function. For $\hbar\omega$ set to 1 eV, VBB-CBD, VBT-CBB, VBT-CBT, and VBT-CBD optical transitions contribute 34.45, 18.62, 14.26, and 32.68 % to the overall JDOS function, respectively.

In Figure 4.4, for the valence band defect model, the fractional contributions of the VBB-CBB, VBB-CBT, VBT-CBB, VBT-CBT, VBD-CBB, and VBD-CBT optical transitions to the overall JDOS function, are plotted as a function of photon energy, $\hbar\omega$. The DOS modeling parameters are set to their nominal a-Si values for the purposes of this analysis, i.e., as set in Table 3.2. The VBB-CBB optical transition contribution to the overall JDOS function is shown with the solid blue line. The VBT-CBB optical transition contribution to the overall JDOS function is shown with the solid green line. The VBB-CBT optical transition contribution to the overall JDOS function is shown with the solid red line. The VBT-CBT optical transition contribution to the overall JDOS function is shown with the solid yellow line. The VBD-CBB optical transition contribution to the overall JDOS function is shown with the solid purple line. The VBD-CBT optical

transition contribution to the overall JDOS function is shown with the light blue line. One should note that, for the selection of $\hbar\omega$ well above the optical gap, i.e., $\hbar\omega > E_{c_{\mathrm{T}}} - E_{v_{\mathrm{T}}}$, the contribution to the overall JDOS function attributable to VBB-CBB optical transitions increases monotonically with increasing $\hbar\omega$, and it is the dominant optical transition in this region while other types of optical transition also contribute. The contribution of the VBB-CBB optical transitions to the overall JDOS function is nil below the optical gap, i.e., $\hbar\omega < E_{c_{\mathrm{T}}} - E_{v_{\mathrm{T}}}$. While VBB-CBT and VBT-CBB optical transitions make small contributions in this region, VBD-CBB and VBD-CBT optical transitions have no contribution to the overall JDOS function in this region. For $\hbar\omega$ set to 2 eV, VBB-CBB, VBB-CBT, and VBT-CBB optical transitions contribute 79.42, 7.05, and 13.53 % to the overall JDOS function, respectively. In the sub-gap region, i.e., $\hbar\omega < E_{c_{\mathrm{T}}} - E_{v_{\mathrm{D}}}$, VBD-CBB optical transitions contribute the most to the overall JDOS function. On the other hand, VBD-CBT and VBT-CBT optical transitions make a small contribution to the overall JDOS. For $\hbar\omega$ set to 1 eV, VBD-CBB and VBD-CBT optical transitions contribute 88.59 and 11.41 % to the overall JDOS function, respectively.

4.3 Comparison with experiment: the conduction band defect model

In this section, results produced through the use of the conduction band defect model, developed earlier in this thesis, are fit to the spectral dependence of the optical absorption coefficient associated with several defect absorption influenced samples of a-Si. Two experimental optical absorption a-Si data sets, and one imaginary part of the dielectric function data set, are considered for the purposes of this analysis. The first set of experimental data points corresponds to the Figure 13(a) of Stolk *et al* [22]. A structure of pure unhydrogenated amorphous silicon was modified by means of ion implantation, furnace annealing, and pulse laser annealing. The sample was annealed for 500 ^{o}C for 1 hour, and is referred to as "relaxed a-Si". The second set of experimental data points corresponds to the "standard GD-a" data points, depicted in Figure 5.2 of Remeš [23]. The sample was prepared by conventional 13.56 MHz glow discharge deposition at a substrate temperature 250 ^{o}C and annealed for 24 hours at 500 ^{o}C to evolve hydrogen. The third set of experimental data points corresponds to the "logarithmic plot of ϵ_2" data points, depicted in Figure 3(b) of Jackson *et al.* [6]. The sample was prepared by doping a 100 nm thick undoped thick film using

2 W rf power and 100 % silane onto a substrate held at 230 ^{o}C. Recalling that the imaginary part of dielectric function

$$\epsilon_2(E) = 4.3 \times 10^{-45} \mathcal{R}^2(E) J(E), \tag{4.1}$$

and the optical absorption coefficient

$$\alpha(E) = \frac{E}{n(E) c \hbar} \epsilon_2(E), \tag{4.2}$$

where $n(E)$ denotes the spectral dependence of the index of refraction, c represents the speed of the light in vacuum, and $\hbar$ is the reduced Plank's constant, one has means of evaluating these optical functions from the JDOS function, $J(E)$. The spectral dependence of the refractive index, $n(E)$, is determined by fitting a tenth-order polynomial to the experimental results of Klazes *et al.* [9]; the experimental data considered for $n(E)$ corresponds to that presented in Figure 4 of Klazes *et al.* [9]; this technique was used previously by Thevaril [4]. It will be assumed that the deviations from this model for $n(E)$ are not significant. Throughout this analysis, $\mathcal{R}^2(E)$ is simply set to 10 Å^2.

A reasonably satisfactory fit with the a-Si experimental data sets of Stolk *et al.* [22] may be achieved by setting $N_{vo} = N_{co} = 2.38 \times 10^{22}$ cm^{-3}eV$^{-3/2}$, $E_v = 0$ eV, $E_c = 1.483$ eV, $E_v - E_{v_{\mathrm{T}}} = 180$ meV, $E_{c_{\mathrm{T}}} - E_c = 25$ meV, $\gamma_v = 105$ meV, $\gamma_c = 60$ meV, $E_{v_{\mathrm{D}}} - E_v = 227$ meV, and $\gamma_{v_{\mathrm{D}}} = 520$ meV.

Table 4.1: The DOS modeling parameter selections for the conduction band defect model associated with a-Si, employed for the purposes of the fit to the experimental data of Stolk *et al.* [22], Remeš [23], and Jackson *et al.* [6]; the corresponding fits are shown in Figures 4.5, 4.6, and 4.7, respectively.

Parameter (unit)	Stolk *et al.* [22]	Remeš [23]	Jackson *et al.* [6]
N_{vo} ($\mathrm{cm}^{-3}\mathrm{eV}^{-3/2}$)	2.38×10^{22}	2.38×10^{22}	2.38×10^{22}
N_{co} ($\mathrm{cm}^{-3}\mathrm{eV}^{-3/2}$)	2.38×10^{22}	2.38×10^{22}	2.38×10^{22}
E_v (eV)	0	0	0
E_c (eV)	1.483	1.59	1.65
$E_v - E_{v_\mathrm{T}}$ (meV)	180	55	55
$E_{c_\mathrm{T}} - E_c$ (meV)	25	35	55
γ_v (meV)	105	76	46
γ_c (meV)	60	43	16
$E_c - E_{c_\mathrm{D}}$ (meV)	227	205	77
γ_{c_D} (meV)	520	590	685

The resultant fit is shown in Figure 4.5. These DOS modeling parameters are tabulated in Table 4.1.

A second reasonably satisfactory fit with the a-Si experimental data sets of Remeš [23] is achieved by setting $N_{vo} = N_{co} = 2.38 \times 10^{22}$ $\mathrm{cm}^{-3}\mathrm{eV}^{-3/2}$, $E_v = 0$ eV, $E_c = 1.59$ eV, $E_v - E_{v_\mathrm{T}} = 55$ meV, $E_{c_\mathrm{T}} - E_c = 35$ meV, $\gamma_v = 76$ meV, $\gamma_c = 43$ meV, $E_{v_\mathrm{D}} - E_v = 205$ meV, and $\gamma_{v_\mathrm{D}} = 590$ meV. The resultant fit is shown in Figure 4.6. These DOS modeling parameters are tabulated in Table 4.1.

The third and last fit was with the a-Si experimental data sets of Jackson *et al.* [6]. A satisfactory fit is achieved by setting $N_{vo} = N_{co} = 2.38 \times 10^{22}$ cm^{-3} $\mathrm{eV}^{-3/2}$, $E_v = 0$ eV, $E_c = 1.65$ eV, $E_v - E_{v_\mathrm{T}} = 55$ meV,

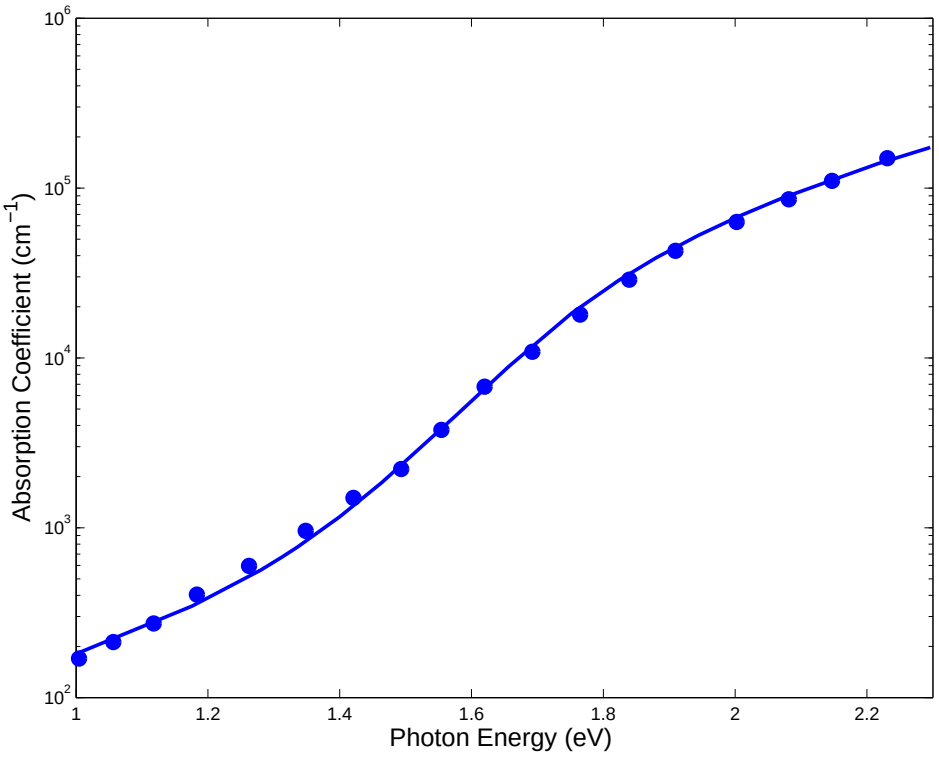

Figure 4.5: The optical absorption spectrum, $\alpha(\hbar\omega)$, associated with a-Si. The experimental a-Si data set of Stolk *et al.* [22] is depicted with solid points; these experimental data points corresponds to the "relaxed a-Si" data points, depicted in Figure 13(a) of Stolk *et al.* [22]. The solid line corresponds the conduction band defect model fitting to this experimental data, by setting the DOS modeling parameters to the selections specified in Table 4.1.

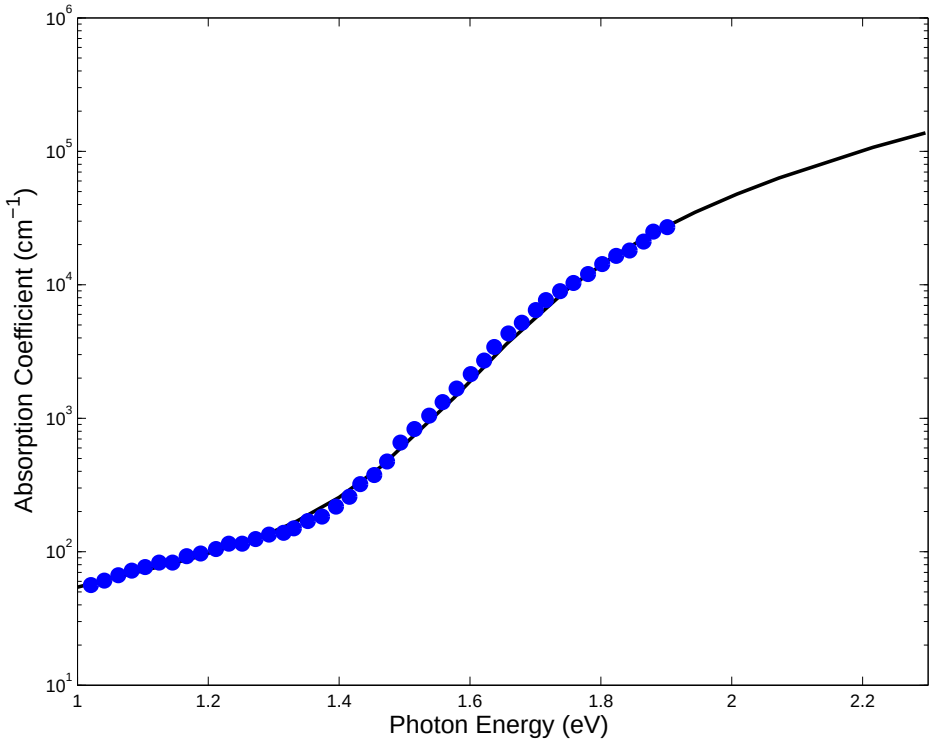

Figure 4.6: The optical absorption spectrum, $\alpha(\hbar\omega)$, associated with a-Si. The experimental a-Si data set of Remeš [23] is depicted with solid points; these experimental data points correspond to the "standard GD-a" data points, depicted in Figure 5.2 of Remeš [23]. The solid line corresponds the conduction band defect model fitting to this experimental data, by setting the DOS modeling parameters to the selections specified in Table 4.1.

$E_{c_T} - E_c = 55$ meV, $\gamma_v = 46$ meV, $\gamma_c = 16$ meV, $E_{v_D} - E_v = 77$ meV, and $\gamma_{v_D} = 685$ meV. The resultant fit is shown in Figure 4.7. The corresponding DOS modeling parameters are also tabulated in Table 4.1.

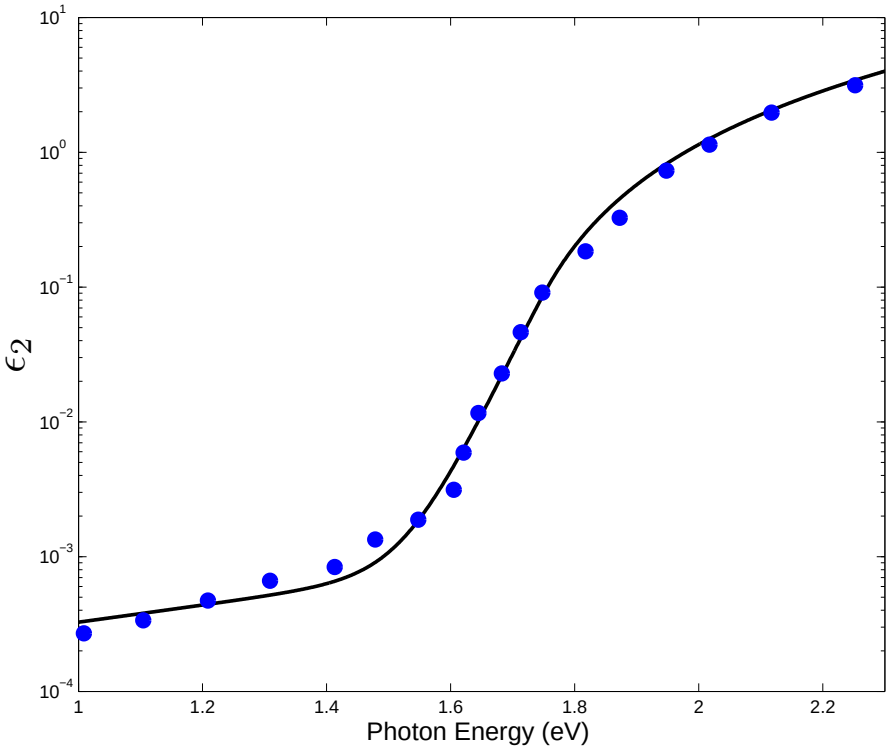

Figure 4.7: The imaginary part of dielectric function spectrum, ϵ_2, associated with a-Si. The experimental a-Si data set of Jackson *et al.* [6] is depicted with solid points; these experimental data points correspond to the "logarithmic plot of ϵ_2" data points, depicted in Figure 3(b) of Jackson *et al.* [6]. The solid line corresponds to the conduction band defect model fitting to this experimental data, by setting the DOS modeling parameters to the selections specified in Table 4.1.

4.4 Comparison with experiment: the valence band defect model

In this section, the valence band defect model developed in this thesis is fit to the spectral dependence of the optical absorption coefficient associated with defect absorption influenced samples of a-Si. As before, two experimental optical absorption a-Si data sets, and one imaginary part of dielectric function data set, are considered for the purposes of this analysis.

A reasonably satisfactory fit with the a-Si experimental data sets of Stolk *et al.* [22] may be achieved by setting $N_{vo} = N_{co} = 2.38 \times 10^{22}$ cm^{-3}eV$^{-3/2}$, $E_v = 0$ eV, $E_c = 1.5$ eV, $E_v - E_{v_\mathrm{T}} = 142$ meV, $E_{c_\mathrm{T}} - E_c = 25$ meV, $\gamma_v = 100$ meV, $\gamma_c = 60$ meV, $E_{v_\mathrm{D}} - E_v = 255$ meV, and $\gamma_{v_\mathrm{D}} = 300$ meV. The resultant fit is shown in Figure 4.8. These DOS modeling parameters corresponding to this fit are tabulated in Table 4.2.

A second reasonably satisfactory fit with the a-Si experimental data sets of Remeš [23] is achieved by setting $N_{vo} = N_{co} = 2.38 \times 10^{22}$ cm^{-3}eV$^{-3/2}$, $E_v = 0$ eV, $E_c = 1.58$ eV, $E_v - E_{v_\mathrm{T}} = 35$ meV, $E_{c_\mathrm{T}} - E_c = 35$ meV, $\gamma_v = 75$ meV, $\gamma_c = 43$ meV, $E_{v_\mathrm{D}} - E_v = 425$ meV, and $\gamma_{v_\mathrm{D}} = 675$ meV. The resultant fit is shown in Figure 4.9. These DOS modeling parameters are tabulated in Table 4.2.

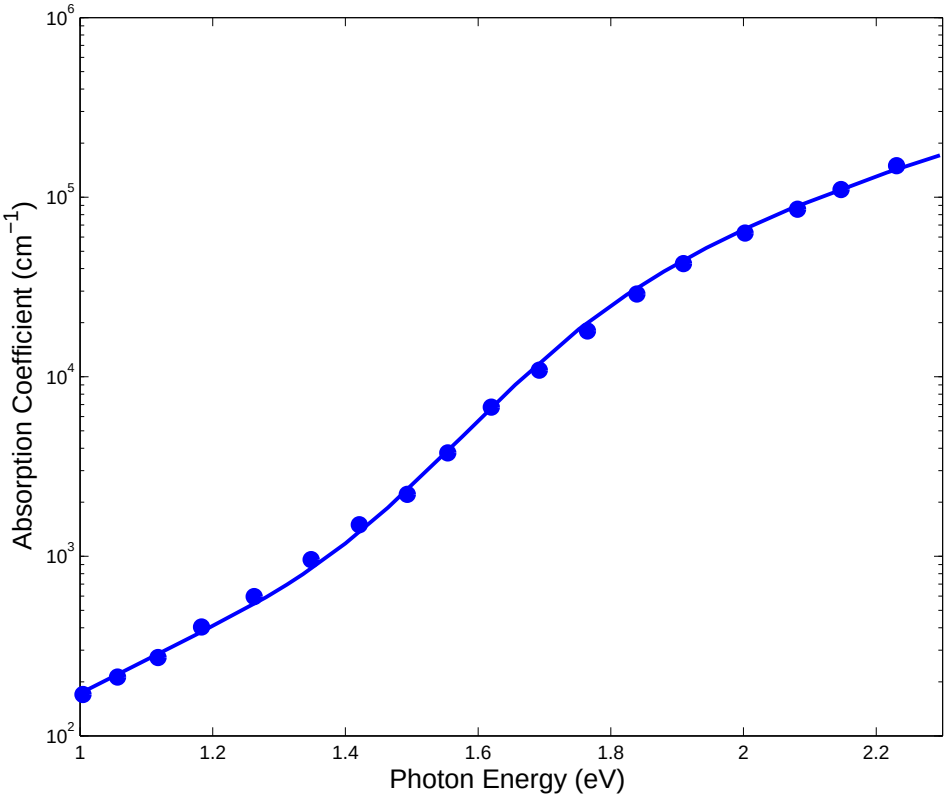

Figure 4.8: The optical absorption spectrum, $\alpha(\hbar\omega)$, associated with a-Si. The experimental a-Si data set of Stolk *et al.* [22] is depicted with solid points; these experimental data points correspond to the "relaxed a-Si" data points, depicted in Figure 13(a) of Stolk *et al.* [22]. The solid line corresponds the valence band defect model fitting to this experimental data, by setting the DOS modeling parameters to the selections specified in Table 4.2.

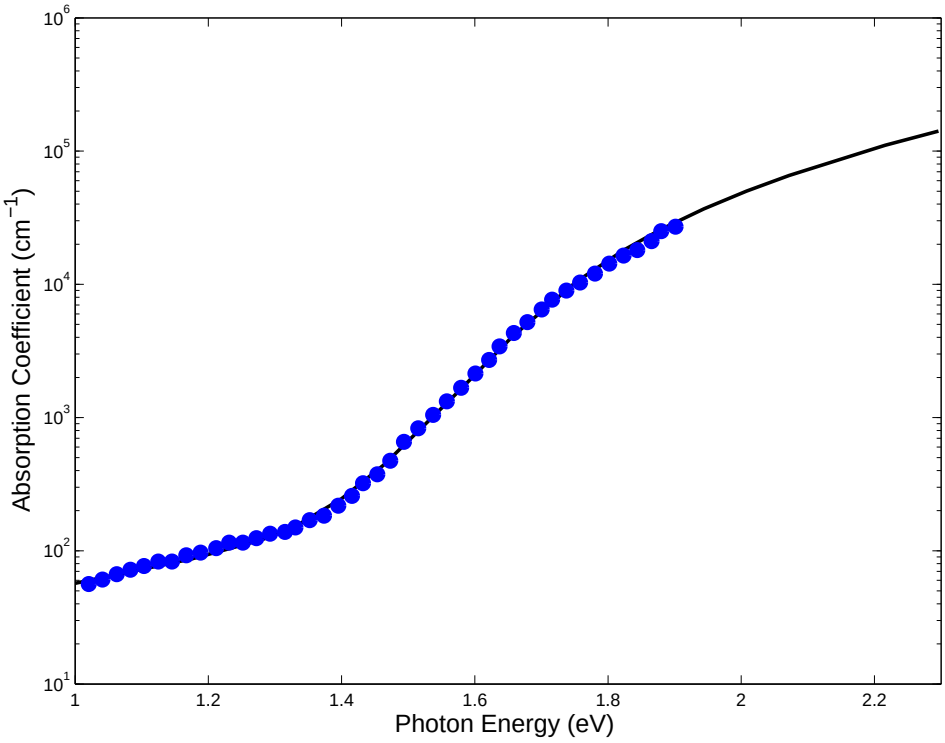

Figure 4.9: The optical absorption spectrum, $\alpha(\hbar\omega)$, associated with a-Si. The experimental a-Si data set of Remeš [23] is depicted with solid points; these experimental data points correspond to the "standard GD-a" data points, depicted in Figure 5.2 of Remeš [23]. The solid line corresponds the valence band defect model fitting to this experimental data, by setting the DOS modeling parameters to the selections specified in Table 4.2.

Table 4.2: The DOS modeling parameter selections for the valence band defect model associated with a-Si, employed for the purposes of the fit to the experimental data of Stolk *et al.* [22], Remeš [23], and Jackson *et al.* [6]; the corresponding fits are shown in Figures 4.8, 4.9, and 4.10, respectively.

Parameter (unit)	Stolk *et al.* [22]	Remeš [23]	Jackson *et al.* [6]
N_{vo} ($\mathrm{cm}^{-3}\mathrm{eV}^{-3/2}$)	2.38×10^{22}	2.38×10^{22}	2.38×10^{22}
N_{co} ($\mathrm{cm}^{-3}\mathrm{eV}^{-3/2}$)	2.38×10^{22}	2.38×10^{22}	2.38×10^{22}
E_v (eV)	0	0	0
E_c (eV)	1.5	1.58	1.68
$E_v - E_{v_\mathrm{T}}$ (meV)	142	35	38
$E_{c_\mathrm{T}} - E_c$ (meV)	25	35	38
γ_v (meV)	100	75	49
γ_c (meV)	60	43	18
$E_{v_\mathrm{D}} - E_v$ (meV)	255	425	340
γ_{v_D} (meV)	300	675	475

The third and last fit was with the a-Si experimental data sets of Jackson *et al.* [6]. A satisfactory fit is achieved by setting $N_{vo} = N_{co} = 2.38 \times 10^{22}$ $\mathrm{cm}^{-3}\mathrm{eV}^{-3/2}$, $E_v = 0$ eV, $E_c = 1.68$ eV, $E_v - E_{v_\mathrm{T}} = 38$ meV, $E_{c_\mathrm{T}} - E_c = 38$ meV, $\gamma_v = 49$ meV, $\gamma_c = 18$ meV, $E_{v_\mathrm{D}} - E_v = 340$ meV, and $\gamma_{v_\mathrm{D}} = 475$ meV. The resultant fit is shown in Figure 4.10. The corresponding DOS modeling parameters are tabulated in Table 4.2.

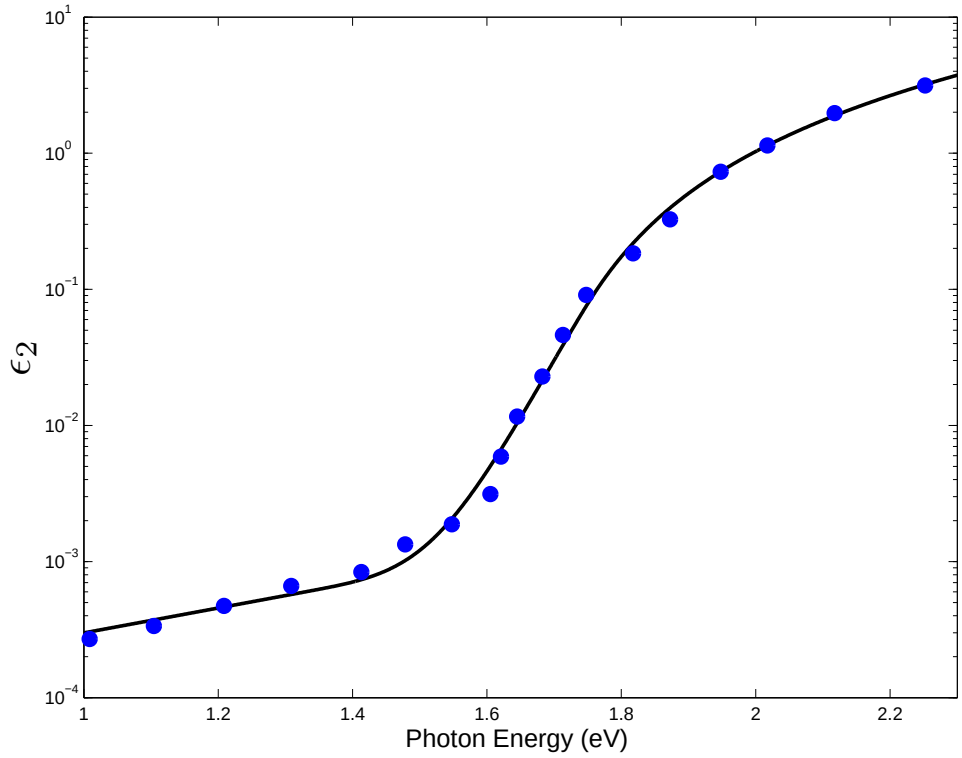

Figure 4.10: The imaginary part of dielectric function spectrum, ϵ_2, associated with a-Si. The experimental a-Si data set of Jackson *et al.* [6] is depicted with solid points; these experimental data points correspond to the "logarithmic plot of ϵ_2" data points, depicted in Figure 3(b) of Jackson *et al.* [6]. The solid line corresponds the valence band defect model fitting to this experimental data, by setting the DOS modeling parameters to the selections specified in Table 4.2.

4.5 On the uniqueness of the fits

The approach that has been adopted for the fitting of the experimental results involved systematically sweeping through a selection of DOS modeling parameter selections until the comparison with experiment is reasonably satisfactory. While this may be adequate for the purposes of this particular analysis, the uniqueness of the fits, i.e., can other selections of DOS modeling parameters produce the similar fits, may be called into question. Further analysis, beyond the scope of the present thesis, will be required in order to resolve this matter.

Chapter 5

Conclusions

In this thesis, empirical models for the DOS functions, that include distributions of defect states, were introduced. Then, the corresponding JDOS functions were evaluated. Through a fit with the results of experiment, the DOS modeling parameters were determined. The fits were found to be satisfactory.

There are a number of topics that are related to this work that could be further explored. The defect model could be further developed to include distributions of defect states associated with both bands. The use of this model for the consideration of other types of amorphous semiconductors would also be a worthwhile pursuit. Developing means of determining the uniqueness of the DOS modeling parameters could also be studied further. The development of formal means of determining the underlying DOS functions from the corresponding optical properties, through the use of this model, would be worthy of further consideration. Finally, what this models

tells one about the design of device that employ these types of materials would also be interesting to examine. These opportunities will have to be explored in the future.

References

[1] W. A. Hadi, "The electron transport within the wide energy gap compound semiconductors gallium nitride and zinc oxide," Ph. D. Thesis, University of Windsor, Windsor, Ontario, Canada, 2014.

[2] "Displays as key driver for large area electronics in intelligent environments: A vision for Europe 2007+", *A proposal for the advancement of the IST thematic priority*, Information Society Technologies, May 2005.

[3] R. A. Street, *Technology and applications of amorphous silicon*, New York: Springer-Verlag, 2000.

[4] J. J. Thevaril, "The optical response of hydrogenated amorphous silicon," Ph. D. Thesis, University of Windsor, Windsor, Ontario, Canada, 2011.

[5] M. Shur, *Introduction to electronic devices*, New York: John Wiley and Sons Inc, 1996.

[6] W. B. Jackson, S. M. Kelso, C. C. Tsai, J. W. Allen, and S.-J. Oh, "Energy dependence of the optical matrix element in hydrogenated amorphous and crystalline silicon," *Physical Review B*, vol. 31, pp. 5187-5198, 1985.

[7] G. D. Cody, B. G. Brooks, and B. Abeles, "Optical absorption above the optical gap of amorphous silicon hydride," *Solar Energy Materials*, vol. 8, pp. 231-240, 1982.

[8] S. K. O'Leary, "An empircal density of states and joint density of states analysis of hydrogenated amorphous silicon: a review," *Journal of Material Science: Materials in Electronics*, vol. 15, pp. 401-410, 2004.

[9] R. H. Klazes and M. H. L. M. van den Broek and J. Bezemer and S. Radelaar, "Determination of the optical bandgap of amorphous silicon," *Philosophical Magazine B*, vol. 45, pp. 377-383, 1982.

[10] S. O. Kasap, *Principles of electronic materials and devices*, 3rd ed. New York: McGraw Hill Higher Education, 2005.

[11] J. Tauc, R. Grigorovici, and A. Vancu, "Optical properties and electronic structure of amorphous germanium," *Physica Status Solidi*, vol. 15, pp. 627-637, 1966.

[12] W. C. Chen, B. J. Feldman, J. Bajaj, F. M. Tong and G. K. Wong, "Thermalization gap excitation photoluminescence and optical absorption in amorphous silicon-hydrogen alloys," *Solid State Communication*, vol. 38, pp. 357-383, 1981.

[13] D. Redfield, "Energy-band tails and the optical absorption edge; the case of a-Si:H," *Solid State Communication*, vol. 44, pp. 1347-1349, 1982.

[14] G. Cody, "The optical absorption edge of a-Si:H," in *Hydrogenated Amorphous Silicon*, ser. Semiconductors and Semimetals, J. I. Pankovepp, Ed. Elsevier, 1984, vol. 21B, pp.11-82.

[15] S. K. O'Leary, S. R. Johnson and P. K. Lim, "The relationship between the distribution of electronic states and the optical absorption spectrum of an amorphous semiconductor: an empirical analysis," *Journal of Applied Physics*, vol. 82, pp. 3334 - 3340, 1997.

[16] J. J. Thevaril and S. K. O'Leary, "A dimensionless joint density of states formalism for the quantitative characterization of the optical response of hydrogenated amorphous silicon," *Journal of Applied Physics*, vol. 107, pp. 083105 1-6, 2010.

[17] M. Shur and M. Hack, "Physics of amorphous silicon based alloy field-effect transistors," *Journal of Applied Physics*, vol. 55, pp. 3831-3842, 1984.

[18] S. M. Malik and S. K. O'Leary, "Optical transitions in hydrogenated amorphous silicon," *Applied Physics Letters*, vol. 80, pp. 790-792, 2002.

[19] J. J. Thevaril and S. K. O'Leary, "Defect absorption and optical transitions in hydrogenated amorphous silicon," *Solid State Communications*, vol. 150, pp. 1851 - 1855, 2010.

[20] S. K. O'Leary, "An analytical density of states and joint density of states analysis of amorphous semiconductors," *Journal of Applied Physics*, vol. 96, pp. 3680-3686, 2004.

[21] S.B. Minar, "An optical functional analysis of amorphous semiconductors", Mater's thesis, University of British Columbia, Canada, 2012.

[22] P. A. Stolk, F. W. Saris, A. J. M. Berntsen, W. F. van der Weg, L. T. Sealy, R. C. Barklie, G. Krotz and G. Muller, "Contribution of defects to electronic, structural, and thermodynamic properties of amorphous silicon," *Journal of Applied Physics*, vol. 75, pp. 7266-7286, 1994.

[23] Z. Remeš, "Study of defects and microstructure of amorphous and microcrystalline silicon thin films and polycrystalline diamond using optical methods," Ph. D. Thesis, Charles University, Prague, 1999.